

Copula-based Sensitivity Analysis for Multi-Treatment Causal Inference with Unobserved Confounding *

Jiajing Zheng
UCSB

Alexander D'Amour
Google Research

Alexander Franks
UCSB

February 19, 2021

Abstract

Recent work has focused on the potential and pitfalls of causal identification in observational studies with multiple simultaneous treatments. On the one hand, a latent variable model fit to the observed treatments can identify essential aspects of the distribution of unobserved confounders. On the other hand, it has been shown that even when the latent confounder distribution is known exactly, causal effects are still not point identifiable. Thus, the practical benefits of latent variable modeling in multi-treatment settings remain unclear. We clarify these issues with a sensitivity analysis method that can be used to characterize the range of causal effects that are compatible with the observed data. Our method is based on a copula factorization of the joint distribution of outcomes, treatments, and confounders, and can be layered on top of arbitrary observed data models. We propose a practical implementation of this approach making use of the Gaussian copula, and establish conditions under which causal effects can be bounded. We also describe approaches for reasoning about effects, including calibrating sensitivity parameters, quantifying robustness of effect estimates, and selecting models which are most consistent with prior hypotheses.

Keywords: Observational studies; multiple treatments; sensitivity analysis; copulas, latent confounders; deconfounder

*Jiajing Zheng is a PhD candidate in the Department of Statistics and Applied Probability at the University of California Santa Barbara (jzheng@pstat.ucsb.edu). Alexander D'Amour is a Research Scientist at Google Research, Cambridge, MA (alexdamour@google.com). Alexander M. Franks is an Assistant Professor of Statistics at the University of California, Santa Barbara (afranks@pstat.ucsb.edu). We thank Steve Yadlowksy, Victor Veitch, and Avi Feller for thoughtful comments and discussion.

1 Introduction

Although it is well-established that treatment effects are not generally identifiable in the presence of unobserved confounding, recent work has focused on whether this challenge can be mitigated when there are multiple simultaneous treatments. Intuitively, dependence among multivariate treatments could provide information about latent confounders, which could in turn be leveraged to facilitate causal inference and identification. This intuition has motivated latent variable approaches such as “the deconfounder”, a much discussed approach for estimating causal effects for multiple treatments (Wang and Blei, 2018).

Unfortunately, it was shown that this strategy has limited practical applicability for point identification and estimation of causal effects. For example, D’Amour (2019a) and D’Amour (2019b) note the lack of general nonparametric identification in the deconfounder approach, and show that the special cases in which the approach does provide identification correspond to situations where all confounding is already observed. Ogburn et al. (2019) and Ogburn et al. (2020) provide several additional counterexamples and detailed rebuttals to previous theoretical results. Even in the special cases where causal effects are identifiable, Grimmer et al. (2020) demonstrate through a suite of simulations and real-data analyses that the deconfounder cannot consistently outperform naive regression. They conclude by further arguing that the deconfounder assumptions are too strong to be applicable in practice.

These challenges are particularly relevant because similar strategies are used in genomics (Price et al., 2006), computational neuroscience, social science and medicine (Zhang et al., 2019), and time series applications (Bica et al., 2020). Given the practical importance of causal inference with multiple treatments, recent work has focused on stronger identifying assumptions for causal effects in the multi-treatment setting. Miao et al. (2020) propose identifying assumptions involving instrumental variables and in settings when over half of the treatments are assumed to have a null effect while Kong et al. (2019) consider identification in a parametric model with binary outcomes.

This literature has revolved around a binary question about point identification: can be causal effects be identified or not? Negative answers to this question often run counter to practitioners’ intuitions in specific data analyses. In particular, it is intuitive that a latent variable model should provide *some* helpful information, even if this information is not enough to fully identify causal effects.

To address this issue, we propose that sensitivity analysis—which explores the range of causal effects that are consistent with the observed data in the context of a given problem—can resolve this tension.

Specifically, sensitivity analysis can show how much is gained by leveraging latent structure in a given application, even if this (usually) falls short of fully identifying the causal effect of interest. To this end, we propose a sensitivity analysis approach to help practitioners better understand confounding in the multi-treatment setting, focusing on the special case where the conditional distribution of unobserved confounders given treatments is identifiable. To extend sensitivity analysis to the multi-treatment setting, we propose a general copula-based decomposition of standard latent variable-based sensitivity analysis models. This factorization allows us to precisely separate the parts of the model that are, and are not, identified in the multi-treatment setting.

For practical analyses, we propose a specialization of the general decomposition, which specifies a sensitivity model based on invariant Gaussian copulas. While this Gaussian copula specification only covers a sub-family of sensitivity models expressible in our general formulation, we show that it captures several essential qualitative aspects of confounding in the multi-treatment setting. In this context, we establish that there are important advantages to multi-treatment inference over single-treatment inference for characterizing sensitivity to unobserved confounding. Specifically, under appropriate assumptions, we establish that the number of effective sensitivity parameters is halved in multi-treatment inference and that this implies that the magnitude of causal effects can be bounded.

The paper proceeds as follows. We begin by defining the relevant quantities and notation in Section 2. In Section 3 we describe our basic framework for latent variable sensitivity analysis via a copula factorization. In Section 4 we introduce a special case of the more general approach in which we assume confounder-outcome relationships can be characterized by a Gaussian copula. In Section 5 we provide some theoretical insights into bias and confounding with the Gaussian copula. We discuss sensitivity parameter interpretation, calibration, and measures of robustness in Section 6 and, finally, in Section 7 and Section 8 we demonstrate our approach in simulation and with the movie example analyzed by Wang and Blei (2018) and later reanalyzed by Grimmer et al. (2020).

2 Preliminaries

2.1 Setup

Let T be a random k -vector of treatment variables, Y be a scalar random outcome of interest, and t and y be realizations of the respective random variables. We let U be a random m -vector denoting unobserved

confounders, and x denote any observed pre-treatment variables. We use the *do*-calculus framework (Pearl, 2009) and let $f(y | do(t))$ denote the density of y in the population in which we have intervened to assign treatment level t to all units. In general, this is distinct from the observed outcome density, $f(y | t)$, which represents the density of the outcome in the subpopulation that received treatment t . These two densities are the same if and only if there are no confounders (VanderWeele and Shpitser, 2013).

The goal of observational inference with multiple treatments is to quantify the effects of different treatments by comparing the intervention distribution at different levels of treatment t (Lechner, 1999; Lopez et al., 2017). In this work we focus on *marginal contrast estimands* (Franks et al., 2019) under arbitrary outcome and treatment distributions. An estimand is a “marginal contrast” if it can be expressed as a function of the marginal distributions of the potential outcomes, $\tau(E[v(y)|do(t_1)], E[v(y)|do(t_2)])$ for some functions v and τ . This includes the vast majority of commonly used estimands. For continuous outcomes, our primary estimand is the difference in the population average outcome for treatment $T = t_1$ and the population average outcome given treatment $T = t_2$:

$$\text{PATE}_{t_1, t_2} := E(Y | do(t_1)) - E(Y | do(t_2)). \quad (1)$$

Here, $v(y) = y$ is the identity function and $\tau(a, b) = a - b$. We also consider the difference in the population average outcome receiving treatment t and observed population average outcome, which we denote

$$\text{PATE}_{t, \cdot} := E(Y | do(t)) - E(Y), \quad (2)$$

where $E(Y) = \int E(Y | t)f(t)dt$ and $\text{PATE}_{t_1, t_2} = \text{PATE}_{t_1, \cdot} - \text{PATE}_{t_2, \cdot}$. The conditional average treatment effects are defined analogously as $\text{CATE}_{t_1, t_2 | x} := E(Y | do(t_1), x) - E(Y | do(t_2), x)$ and $\text{CATE}_{t, \cdot | x} := E(Y | do(t), x) - E(Y | x)$.

For binary outcomes, our primary estimand is the causal risk ratio between treatments t_1 and t_2

$$\text{RR}_{t_1, t_2} = P(Y = 1 | do(t_1)) / P(Y = 1 | do(t_2)). \quad (3)$$

where $\text{RR}_{t, \cdot}$ is defined analogously to (2), as $P(Y = 1 | do(t)) / P(Y = 1)$, so that we can express $\text{RR}_{t_1, t_2} = \text{RR}_{t_1, \cdot} / \text{RR}_{t_2, \cdot}$. Here $v(y) = I[y = 1]$ is the indicator function and $\tau(a, b) = a/b$.

In general, it is difficult to infer PATEs or RRs from observational data since the potential presence of

unmeasured confounders, which affect both treatment and outcome, can bias naive estimates. If U were to be observed, the following assumptions would be sufficient to identify the intervention distribution, and hence the treatment effect:

Assumption 1 (Latent ignorability). X and U block all backdoor paths between T and Y (Pearl, 2009).

Assumption 2 (Positivity). $f(T = t | U = u, x) > 0$ for all u and x .

Assumption 3 (SUTVA). There are no hidden versions of the treatments and there is no interference between units (see Rubin, 1980).

Since u is not observed, and x alone does not block all backdoor paths, then treatment effects are not identifiable without additional assumptions. In this case, a common solution is to conduct a sensitivity analysis which characterizes how the implied causal effects change under different assumptions about U and its relationship to T and Y .

2.2 Sensitivity Analysis

There is an extensive literature on assessing sensitivity to violations of unconfoundedness in single treatment models, dating back at least to the work of Cornfield et al. (1959) on the link between smoking and lung cancer. Since then, a wide range of strategies have been proposed for assessing sensitivity to unobserved confounding (e.g. see Greenland, 1996; Gastwirth et al., 1998; Vansteelandt et al., 2006; Imbens, 2003; VanderWeele and Arah, 2011; VanderWeele et al., 2012; Robins et al., 2000; Franks et al., 2019; Cinelli and Hazlett, 2019; Veitch and Zaveri, 2020). A common strategy for sensitivity analysis is to assert, as in Assumption 1, that unconfoundedness would hold if only an additional latent variable U were observed (Rosenbaum and Rubin, 1983). With assumptions 1 and 2, latent confounder models simultaneously specify the full conditional distributions of treatment and outcomes given both observed confounders, x , and unobserved confounders, U . The dependence of Y and T on U is indexed by a vector of sensitivity parameters $\psi = (\psi_Y, \psi_T)$. Practitioners can then reason about how assumptions about these parameters translate to different causal conclusions. Often, this is done through *calibration*, by determining reasonable ranges for ψ using analogies about observable associations and through a *robustness* assessment, by examining how strong associations with unobserved confounders must be for conclusions to change.

Concretely, in a typical latent confounder analysis, we posit densities $f(u | x)$, the marginal density of the latent confounders, $f_{\psi_T}(t | x, u)$, the conditional density (or PMF) for treatment assignment given all

confounders and $f_{\psi_Y}(y | x, u, t)$, the outcome density in treatment arm t . The sensitivity parameters encode the relationship between both the treatment and unobserved confounders and the outcome and unobserved confounders (e.g. see [Imbens, 2003](#); [Dorie et al., 2016](#)). Latent confounder models are usually parameterized so that some specific values of the sensitivity parameters ψ indicate the “no unobserved confounding” case. For example, we can take $\psi_T = 0$ to imply that $f_{\psi_T}(t | x, u) = f_{\psi_T}(t | x)$ and $\psi_Y = 0$ to imply that $f_{\psi_Y}(y | x, u, t) = f_{\psi_Y}(y | x, t)$. Then, when either $\psi_T = 0$ or $\psi_Y = 0$, U is not a confounder ([VanderWeele and Shpitser, 2013](#)). Without loss of generality, we suppress conditioning on x throughout the remainder of the manuscript, and comment on the role of observed covariates where appropriate.

A key principle of sensitivity analysis is that the observed data densities should be invariant to the sensitivity parameters ([Gustafson et al., 2018](#)). Unfortunately, this principle can easily be violated in a latent confounder analysis ([Franks et al., 2019](#)). The crux of the problem is that, in general, none of $f(u | x)$, $f_{\psi_T}(t | x, u)$ or $f_{\psi_Y}(y | x, u, t)$ are nonparametrically identifiable themselves, but the observed outcome density, which is a function of these densities, is identifiable. The observed outcome density, has the following form:

$$f(y | T = t) = \int_{\mathcal{U}} f_{\psi_Y}(y | t, u) f_{\psi_T}(u | t) du, \text{ for all } t \text{ and } \psi \quad (4)$$

where $f_{\psi_T}(u | t)$ is the conditional density of the latent confounders given treatment level t . This contrasts with the density of the intervention distribution, which is:

$$f_{\psi}(y | do(t)) = \int_{\mathcal{U}} f_{\psi_Y}(y | t, u) f(u) du \quad (5)$$

$$= \int_{\mathcal{U}} f_{\psi_Y}(y | t, u) \left[\int f_{\psi_T}(u | \tilde{t}) f(\tilde{t}) d\tilde{t} \right] du \quad (6)$$

The intervention distribution is obtained by integrating over the marginal distribution of the unobserved confounder, $f_{\psi_T}(u) = \int f_{\psi_T}(u | \tilde{t}) f(\tilde{t}) d\tilde{t}$, whereas the observed data distribution in 4 is obtained by integrating with respect to the conditional confounder distribution, $f_{\psi_T}(u | t)$. A fundamental challenge of sensitivity analysis is to specify a class of densities $f_{\psi_Y}(y | t, u)$ and $f_{\psi_T}(u | t)$, with interpretable parameters $\psi = (\psi_Y, \psi_T)$, for which the intervention distribution necessarily varies with ψ but for which the observed data distribution does not.

In fact, several authors have proposed latent variable sensitivity models with unidentified sensitivity parameters in single-treatment settings. Many of these are in simple settings with binary or categorical

outcomes (Rosenbaum and Rubin, 1983; Robins, 1997; Vansteelandt et al., 2006; Daniels and Hogan, 2008). A more general solution was proposed by Zhang and Tchetgen (2019) who propose a semi-parametric sensitivity model in which the distribution of U is left unrestricted. Franks et al. (2019) propose an alternative framework for sensitivity analysis without directly introducing latent variables by directly parameterizing the effect of the outcome on the treatment assignment. Cinelli and Hazlett (2019) and Cinelli et al. (2019) use moment arguments to derive confounding bias in the linear regression setting and introduce an approach for sensitivity parameter calibration based on the proportion of variance explained by the latent confounder. In the multiple treatment setting, additional observable implications can complicate sensitivity analysis, and thus new strategies are needed. Below, we describe our copula based approach for addressing this challenge.

3 Sensitivity Analysis via Copula Parameterizations

The multiple treatment setting presents unique challenges for sensitivity analysis. In particular, the additional structure imposed in studies with multiple treatments introduces new observable implications, muddling issues of identifiability. We focus on the specific case in which the conditional confounder distribution $f_{\psi_T}(u | t)$ may be partially identifiable from the multiple treatments. To adapt sensitivity analysis to this setting, sensitivity parameters must not only be decoupled from the observed data distribution; parameters describing the treatment-confounder relationships must also be decoupled from parameters describing the outcome-confounder relationships. We tackle this challenge by factorizing the joint distribution $f(y, u, t)$ using a copula, which decompose joint distributions of variables into their marginal distributions and joint dependence.

In this section, we introduce our copula-based factorization, discuss how it applies to the multiple treatment setting, and then discuss the Gaussian copula parameterization, a special case that we will use in theoretical analysis and methods development in the remainder of the paper.

3.1 General Copula-Based Formulation

Our approach is based on the following factorization. The model for Y conditional on treatments and unobserved confounders can be decomposed into the observed data density and a conditional copula as

$$f_{\psi}(y | u, t) = f(y | t)c_{\psi_Y}(F_{Y|t}(y), F_{U|t}^{\psi_T}(u) | t) \tag{7}$$

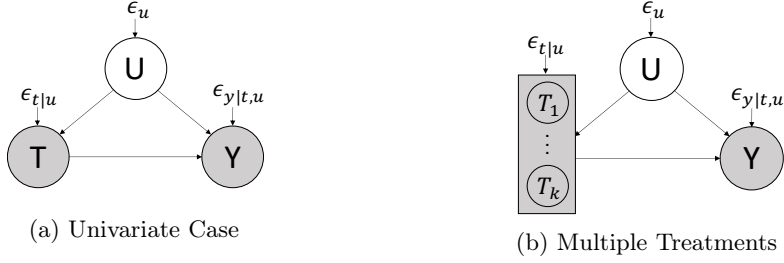


Figure 1: Treatment T , outcome Y , unobserved variables U . ϵ_u , $\epsilon_{t|u}$ and $\epsilon_{y|t,u}$ are respectively the random noises of U , T and Y .

where $F_{Y|t}$ is the CDF of $f(y | t)$ and $F_{U|t}$ is the CDF of $f_{\psi_T}(u | t)$. c_{ψ_Y} is the conditional copula density, defined on the unit hypercube and parameterized by ψ_Y , which characterizes the joint density of Y and U conditional of $T = t$ after transforming the marginals to uniform random variables (Nelsen, 2007). By explicitly factoring the observed outcome density, $f(y | t)$, out of the complete data distribution, we ensure that the left hand side of Equation 4 is invariant to ψ , establishing that there are no observable implications of varying the copula parameters. Moreover, this factorization holds for all densities (or PMFs) $f(y | t)$ and $f_{\psi_T}(u | t)$ and any number of treatments, and thus can be used to characterize the outcome-confounder dependence for any model of the observables.

With Equation 7, we can express the intervention distribution, $f_\psi(y | do(t))$, as:

$$f_\psi(y | do(t)) = f(y | t) \int c_{\psi_Y}(F_{Y|t}(y), F_{U|t}^{\psi_T}(u) | t) f(u) du, \quad (8)$$

$$= f(y | t) \int c_{\psi_Y}(F_{Y|t}(y), F_{U|t}^{\psi_T}(u) | t) \left[\int f_{\psi_T}(u | \tilde{t}) f(\tilde{t}) d\tilde{t} \right] du \quad (9)$$

The observed outcome distribution $f(y | t)$ and the marginal distribution of treatment $f(t)$ are clearly invariant to the sensitivity parameters by construction. The intervention distribution $f(y | do(t))$ is parameterized by ψ_Y , the parameter governing the conditional dependence between Y and U given T and by ψ_T , the parameters governing the conditional distribution of U given T .

Given $f(y | t)$, $f_{\psi_T}(u | t)$ and c_{ψ_Y} we can compute the expected value of any function of the outcome under the intervention distribution, $E[v(Y) | do(t)] = \int v(y) f(y | do(t)) dy$. This can be in turn used to compute any marginal contrast estimand. By applying Equation 8, we write this intervention expectation as

$$E[v(Y) | do(t)] = \int v(y) w_\psi(y, t) f(y | t) dy, \quad (10)$$

where $w_\psi(y, t) = \int c_{\psi_Y}(F_{Y|t}(y), F_{U|t}^{\psi_T}(u) | t) f_{\psi_T}(u) du$ is the importance weight associated with sampling from the observed data distribution instead of the intervention distribution. In practice, we can approximate the marginal distribution of the unobserved confounder with the mixture density $f_{\psi_T}(u) \approx \frac{1}{n} \sum_i f^{\psi_T}(u | t_i)$ where $t_i \in \mathcal{T}$ is the i th observed treatment and \mathcal{T} is the set of all observed treatment vectors. Thus, the importance weight can be approximated as

$$w_\psi(y, t) \approx \frac{1}{|\mathcal{T}|} \sum_{t_i \in \mathcal{T}} \left[\int c_{\psi_Y}(F_{Y|t}(y), F_{U|t}^{\psi_T}(u) | t) f_{\psi_T}(u | t_i) du \right]. \quad (11)$$

We use this approximation to derive importance sampling algorithm for computing the the expected value in Equation 10 for any copula and conditional confounder distributions $f(u | t)$ (Appendix, Algorithm 2). This can in turn be used to compute any marginal contrast estimand, $\tau(E[v(y)|do(t_1)], E[v(y)|do(t_2)])$.

3.2 Multiple Treatments and Causal Equivalence Classes

Algorithm 2 is fully general and thus can be used to compute marginal contrast estimands in a single treatment setting, multiple treatment setting, or even multiple outcome settings. However, the primary motivation in this paper is to study this factorization in multiple treatments setting when there additional observable implications from latent variable models. The copula factorization elucidates the role of confounding even when aspects of the treatment-confounder relationship are identifiable from multiple treatments. Specifically, with multiple treatments, the conditional distribution of latent confounders given treatments, parameterized by ψ_T , is often identifiable up to a particular equivalence class (e.g. up to rotation and scale).

In this paper, we focus on inference with latent variable methods where ψ_T is identified up to an equivalence class where the set of possible causal effects compatible with any particular value of ψ_T does not change within this class. We formalize this notion through the following definition and assumption.

Definition 1 (Causal equivalence class). $[\psi_T]$ is a causal equivalence class of ψ_T if and only if for any $\tilde{\psi}_T$ in $[\psi_T]$, then, for every ψ_Y there exists a $\tilde{\psi}_Y$ such that $f_{\psi_Y, \psi_T}(y | do(T = t)) = f_{\tilde{\psi}_Y, \tilde{\psi}_T}(y | do(T = t))$ for all y, t .

For the purposes of sensitivity analysis, when ψ_T is identified up to a causal equivalence class, we can assume that ψ_T is point-identified at a particular value within the class $[\psi_T]$ without loss of generality. Identification up to a causal equivalence class is not generally possible in single treatment studies but will often hold in a multi-treatment study when certain identifying conditions for the latent variable model are

met.

Crucially, the copula-based formulation enables valid sensitivity analysis without observable implications, even in these cases where ψ_T is restricted by the observed data. In this case, the outcome-confounder copula c_{ψ_Y} remains the lone degree of freedom in the sensitivity model. As we will show, this restriction can induce qualitatively different sensitivity regions in the multi-treatment setting as opposed to the single-treatment setting. For example, sensitivity regions can be bounded, even without additional restrictions on ψ_Y .

4 Practical Sensitivity Analysis with the Gaussian Copula

In practice, it is infeasible to characterize and interpret the implied causal effects for all possible copula specifications. In this section, we propose a practical sensitivity analysis method based on the special case in which c_{ψ_Y} is a Gaussian copula. This model characterizes the sensitivity of causal effects to monotone dependencies between the outcome and unobserved confounders. As we will discuss in the following sections, the Gaussian copula facilitates interpretation and sensitivity parameter calibration, and, as before, is compatible with arbitrary marginal distributions $f(y | t)$ and $f(t)$. For our method and throughout the remainder of the paper we make the following additional assumptions:

Assumption 4 (Copula invariance). The conditional copula does not depend on the value of t , that is, the conditional dependence between Y and U is invariant to the level of T .

Assumption 5 (Gaussian copula). The conditional copula between the outcome and m -dimensional latent confounders given treatments, $c_{\psi}(F_{Y|t}(y), F_{U|t}(u) | t)$, is a Gaussian copula.

These assumptions do not impose constraints on the observed data distributions, only the relationship between the observed and latent variables. Given Assumption 4 and 5, the conditional confounder density can be expressed as a multivariate normal density, $f(u | t) \sim N(\mu_{u|t}, \Sigma_{u|t})$, where $\Sigma_{u|t}$ invariant to the level of t . Together, these assumptions imply the following generative model:

$$T \sim F_T \tag{12}$$

$$f(u | t) \sim N(\mu_{u|t}, \Sigma_{u|t}) \tag{13}$$

$$\tilde{Y} = \gamma'(U - \mu_{u|t}) + \epsilon_{\tilde{y}|t,u}, \quad \epsilon_{\tilde{y}|t,u} \sim N(0, \sigma_{\tilde{y}|t,u}^2), \quad \gamma^T \Sigma_{u|t} \gamma + \sigma_{\tilde{y}|t,u}^2 = 1 \tag{14}$$

$$Y = F_{Y|t}^{-1}(\Phi(\tilde{Y})) \tag{15}$$

where F_T is the distribution of the treatments and $F_{Y|t}^{-1}$ is the inverse-CDF of the conditional distribution of Y given $T = t$. The Gaussian copula is parameterized by the correlation matrix implied by

$$\text{Cov}([\tilde{Y}, U] | T = t) = \begin{bmatrix} 1 & \gamma^T \Sigma_{u|t} \\ \Sigma_{u|t} \gamma & \Sigma_{u|t} \end{bmatrix}. \quad (16)$$

with parameters are $\psi_T = \{\mu_{u|t}, \Sigma_{u|t}\}$ and $\psi_Y = \{\gamma\}$. In general, $\mu_{u|t}$ and $\Sigma_{u|t}$ will not be point identified, although under many latent variable models they can be identified up to invertible linear transformation of U . Importantly, the following theorem establishes that the class of ψ_T defined by all invertible linear transformations of U is a causal equivalence class.

Theorem 1. *Assume model 13-15. Let $[\psi_T] = \{\tilde{\psi}_T = \{A\mu_{u|t}, A\Sigma_{u|t}A\} : A \in \mathcal{S}^+\}$ where \mathcal{S}^+ is the space of symmetric positive definite matrices. Then $[\psi_T]$ is a causal equivalence class.*

The gist of the proof is that for any invertible linear transformation, A , of U , the copula parameterized by $\tilde{\gamma} = A^{-1}\gamma$ yields equivalent causal effects in the reparameterized coordinates of U as γ does in the original confounder coordinates.

Throughout this work, we will assume that ψ_T is identified up to invertible linear transformations of U , and explore the range of possible causal effects for different γ satisfying $\gamma^T \Sigma_{u|t} \gamma \leq 1$. In Algorithm 1, we provide a procedure for estimating any marginal contrast estimand, given a sensitivity vector γ and treatments levels t_1 and t_2 . At a high level, we compute a Monte Carlo estimate of $f(y | do(t))$ via the following three step procedure: 1) draw a sample from $f(u)$, 2) compute the conditional density of of the Gaussianized outcome $f(\tilde{Y} | u, t)$ via the Gaussian copula and 3) transform \tilde{Y} back to original space via the conditional quantile function $F_{Y|t}^{-1}$ (see Figure 3). In the following Sections, we introduce some theoretical insights about our approach and also provide a method for calibrating the magnitude of γ and reasoning about it's direction.

5 The Geometry of Sensitivity in the Gaussian Copula Model

As described in the previous Section, our method for practical sensitivity analysis with multiple treatments is based on a Gaussian copula parameterization of the confounder-outcome relationship. Here, we start by providing some theoretical insights about how the Gaussian covariance structure relates to confounding bias in the linear-Gaussian model. Specifically, we describe how the causal effects vary as a function of γ and how

Algorithm 1 Marginal Contrast Estimation.

```
1: function COMPUTEMEAN( $t, \gamma$ )
2:   for  $i = 1, 2, \dots, n$  do
3:      $\mu_i \leftarrow \gamma^T(\mu_{u|t_i} - \mu_{u|t})$ 
4:     for  $j = 1, 2, \dots, nSim$  do
5:       Sample  $\tilde{y}_{ij}$  from  $N(\mu_i, 1)$ 
6:        $y_{ij} \leftarrow F_{Y|t}^{-1}(\Phi(\tilde{y}_{ij}))$ 
7:     end for
8:   end for
9:   return  $\frac{1}{n} \sum_{ij} v(y_{ij})$ 
10: end function
11: Return  $\tau(\text{ComputeMean}(t_1, \gamma), \text{ComputeMean}(t_2, \gamma))$ 
```

bounds on these effects depend on both the treatment contrast and inferred conditional confounder density. In 5.2, we generalize some of these results to arbitrary models for $f(y | t)$ and $f(t)$.

5.1 Confounding Bias in the Linear-Gaussian Model

We start by illustrating our approach in a simple Linear-Gaussian model when (Y, T, U) are jointly multivariate Gaussian and establish the following results:

- For causal inference with a single treatment, the confounding bias for PATE_{t_1, t_2} is unbounded.
- When there are multiple treatments which can be used to identify (up to a causal equivalence class) the conditional confounder distribution, the magnitude of the confounding bias for PATE_{t_1, t_2} is bounded. We characterize how the magnitude of this bound depends on the parameters of the latent confounder model.
- In the multi-cause setting there are many possible treatment contrasts. The confounding bias depends on the contrast. We characterize which treatment contrasts lead to the largest bounds and which treatment contrasts imply identifiable effects.

We demonstrate these results in the following model:

$$U = \epsilon_u, \quad \epsilon_u \sim N_m(0, \Sigma_u), \tag{17}$$

$$T = BU + \epsilon_{t|u}, \quad \epsilon_{t|u} \sim N_k(0, \sigma_{t|u}^2 I_k), \tag{18}$$

$$Y = \tau' T + \gamma' U + \epsilon_{y|t,u}, \quad \epsilon_{y|t,u} \sim N_m(0, \sigma_{y|t,u}^2), \tag{19}$$

with $\tau \in \mathbb{R}^k$ and $\gamma \in \mathbb{R}^m$. When either $B = 0$ or $\gamma = 0$, there is no confounding. We also note that Equations 17 and 18 imply that the conditional distribution of the confounder can be expressed as $f(u | t) \sim N(\mu_{u|t}, \Sigma_{u|t})$, as in Equation 13, where both $\mu_{u|t}$ and $\Sigma_{u|t}$ are known functions of B and $\sigma_{t|u}^2$. Under model 17-19, the intervention distribution has density

$$f(y | do(T = t)) \sim N(\tau't, \sigma_{y|t,u}^2 + \gamma'\Sigma_u\gamma). \quad (20)$$

For any t_1, t_2 , PATE_{t_1, t_2} is characterized entirely by the regression coefficients τ . The observed outcome distribution can be expressed as

$$f(y | T = t) \sim N(\tau'_{\text{naive}}t, \sigma_{y|t}^2) \quad (21)$$

where

$$\tau_{\text{naive}} = \tau + (B\Sigma_u B' + \sigma_{t|u}^2 I_k)^{-1} B\Sigma_u \gamma \quad (22)$$

$$\sigma_{y|t}^2 = \sigma_{y|t,u}^2 + \gamma'(\Sigma_u - \Sigma_u B'(B\Sigma_u B' + \sigma_{t|u}^2 I_k)^{-1} B\Sigma_u)\gamma \quad (23)$$

$$= \sigma_{y|t,u}^2 + \gamma'\Sigma_{u|t}\gamma \quad (24)$$

which are both fully identified from observed data. We refer to τ_{naive} as the naive estimate since it naively neglects the effect of unobserved confounders. Equation 24 shows that the observed residual outcome variance can be decomposed into nonconfounding variation $\sigma_{y|t,u}^2$ and confounding variation, $\gamma'\Sigma_{u|t}\gamma$. We take $\sigma_{y|t}^2$ and τ_{naive} as fixed and known, and characterize the range of confounding biases by considering different assumptions about the strength of confounding.

We note that the bias of the naive estimator depends only on the difference between the treatment vectors, $\Delta t = t_1 - t_2$, since the population average treatment effect can be expressed as

$$\text{PATE}_{\Delta t} = \tau'(t_1 - t_2) := \tau'\Delta t, \quad (25)$$

The confounding bias, denoted $\text{Bias}_{\Delta t} = \tau'_{\text{naive}} \Delta t - \text{PATE}_{\Delta t}$, can then be expressed as

$$\text{Bias}_{\Delta t} = \gamma' \Sigma_u B' (B \Sigma_u B' + \sigma_{t|u}^2 I_k)^{-1} \Delta t \quad (26)$$

$$= \gamma' (E(U | T = t_1) - E(U | T = t_2)) \quad (27)$$

$$:= \gamma' \mu_{u|\Delta t}, \quad (28)$$

where we use $\mu_{u|\Delta t}$ to denote the difference in confounder means for the treatment contrast, Δt . We can then succinctly express the PATE in terms of the naive estimate minus the bias as $\text{PATE}_{\Delta t} = \tau_{\text{naive}}' \Delta t - \gamma' \mu_{u|\Delta t}$.

In the single treatment setting, neither $\psi_Y = \{\gamma\}$ nor $\psi_T = \{\mu_{u|\Delta t}, \Sigma_{u|t}\}$ are identifiable, which implies that the confounding bias is unbounded. However, with multiple treatments ψ_T is identifiable up to a causal equivalence class defined by invertible linear transformations of U . We make this concrete in the following theorems.

Theorem 2. *Suppose that the observed data is generated by model 17-19. When there k treatments with $1 < m < k$, then ψ_T is identified up to the causal equivalence class $[\psi_T] = \{\tilde{\psi}_T = \{A\mu_{u|t}, A\Sigma_{u|t}A\} : A \in \mathcal{S}^+\}$. When there is a single treatment ($k = 1$) or at least $m = k$ confounders, then ψ_T is not identifiable up to causal equivalence class.*

Proof. See appendix.

One consequence of Theorem 2 is that the distribution of U is only causally relevant up to linear transforms, and as such, without loss of generality, we make the simplifying assumption that $U \sim N(0, I_m)$ for the remainder of this Section.

First, we review the implications of this theorem when there is only a single treatment, i.e. $k = 1$. As shown in Cinelli and Hazlett (2019), for single treatment inference, the squared confounding bias of the PATE can be expressed as

$$\text{Bias}_{\Delta t}^2 = \frac{R_{T \sim U}^2}{1 - R_{T \sim U}^2} R_{Y \sim U|T}^2 \frac{\sigma_{y|t}^2}{\sigma_T^2} \quad (29)$$

where $\sigma_T^2 := BB' + \sigma_{t|u}^2 I_k$ is the marginal variance of the treatment,

$$0 \leq R_{T \sim U}^2 = \frac{\sigma_T^2 (\mu_{u|\Delta t})' \mu_{u|\Delta t}}{(\Delta t)^2} \leq 1 \quad (30)$$

is the unidentified fraction of treatment variance explained by confounders and

$$0 \leq R_{Y \sim U|T}^2 = \frac{\gamma^T \Sigma_{u|t} \gamma}{\sigma_{y|t}^2} \leq 1 \quad (31)$$

is the fraction of the residual outcome variance explained by confounders. By Theorem 2, neither $R_{T \sim U}^2$ nor $R_{Y \sim U|T}^2$ are identifiable. Since $\frac{R_{T \sim U}^2}{1 - R_{T \sim U}^2}$ can be arbitrarily large, the confounding bias is unbounded in the single treatment setting.

In contrast, Theorem 2 states that with multiple treatments, we can identify an element of the causal equivalence class for parameters governing the conditional confounder distribution. The relationship between Y and U , as parameterized by m-vector γ , remains an unidentified sensitivity vector. This sensitivity vector can be viewed as parameterizing the Gaussian conditional copula between Y and U given T , $c_\gamma(F_{Y|t}(y), F_{U|t}(u) | t)$ (Equation 16).

Identification up to causal equivalence class implies that the confounding bias is bounded. From Equation 26, we can see that the sign and magnitude of the bias depends on both Δt as well as γ . Although γ is not identified, its values are constrained since unobserved confounding cannot explain more than 100% of the residual outcome variance (Equation 31). This constraint on the magnitude of γ implies the following result about the bias of the naive estimator.

Theorem 3. *Suppose that the observed data is generated by model 17-19 with $\sigma_{t|u}^2 > 0$. Then, $\forall \gamma$ satisfying Assumptions 1 and 2,*

$$\gamma^T \Sigma_{u|t} \gamma \leq \sigma_{y|t}^2 \quad (32)$$

For any given Δt , we have

$$Bias_{\Delta t}^2 \leq \sigma_{y|t}^2 R_{Y \sim U|T}^2 \|\Sigma_{u|t}^{-1/2} \mu_{u|\Delta t}\|_2^2, \quad (33)$$

The bound is achieved when γ is colinear with $\Sigma_{u|t}^{-1} \mu_{u|\Delta t}$.

Proof. See appendix.

This theorem states that the true causal effect lies in the interval $\tau'_{naive} \Delta t \pm \sqrt{\sigma_{y|t}^2 R_{Y \sim U|T}^2 \|\Sigma_{u|t}^{-1/2} \mu_{u|\Delta t}\|_2}$. When additional assumptions are applied to identify a particular value of γ (e.g. see Miao et al., 2020), the corresponding causal effect estimate will correspond to a single point inside this ignorance region when the Gaussian copula assumption holds. We refer to the right-hand side of 33 as the “worst-case bias” of the naive estimator. In particular, since τ_{naive} is the midpoint of the ignorance region, it has the minimum worst-case

bias over all alternative causal effect estimators. This is consistent with [Grimmer et al. \(2020\)](#) who emphasize that the deconfounder proposed by [Wang and Blei \(2018\)](#) cannot outperform the naive estimator in general.

The worst-case bias of τ_{naive} is proportional to the norm of the scaled difference in confounder means in each treatment arm, $\Sigma_{u|t}^{-1/2} \mu_{u|\Delta t}$. This result provides a useful generalization of existing work which demonstrates that overlap is violated when u can be pinpointed by a deterministic function of t ([D’Amour, 2019b](#)). In contrast to the original work by [Wang and Blei \(2018\)](#), our result suggests that the more precisely we can pinpoint u given t , the *less* precisely we can pinpoint $\text{PATE}_{\Delta t}$. In the following corollary, we state the worst-case bias over all possible treatment contrasts:

Corollary 3.1. *Let d_1 be the largest singular value of B . For all Δt with $\|\Delta t\|_2 = 1$, the squared bias is bounded by*

$$\text{Bias}_{\Delta t}^2 \leq \frac{d_1^2}{(d_1^2 + \sigma_{t|u}^2)} \frac{\sigma_{y|t}^2}{\sigma_{t|u}^2} R_{Y \sim U|T}^2, \quad (34)$$

with equality when $\Delta t = u_1^B$, the first left singular vector of B . When $\Delta t \in \text{Null}(B')$, the naive estimate is unbiased, that is, $\text{PATE}_{\Delta t} = \tau'_{\text{naive}} \Delta t$.

Proof: See Appendix.

The first term in (67), $\frac{d_1^2}{(d_1^2 + \sigma_{t|u}^2)}$, is the fraction of variance in the first principal component of the causes that can be explained by confounding. The first principal component corresponds to the projection of treatments which is most correlated with confounders, and thus is the causal contrast with the largest ignorance region. We also note that the squared biases depends on $R_{Y \sim U|T}^2$, the partial variance explained by confounders given treatments. While the magnitude of the confounding bias is always largest when $R_{Y \sim U|T}^2 = 1$, we often have reason to believe that the variance explained by confounders is likely smaller. We describe how to leverage this idea to calibrate more plausible bounds and measures of robustness in Section 6.

We illustrate some key insights from these theorems in Figure 2, where we display the worst-case bias as a function of the treatment contrasts, Δt . In this illustration, we assume that Δt lies on a plane spanned by u_1^B and n_0^B , an arbitrary vector in the null space of B . We let $\theta = \arccos(\Delta t' u_1^B)$ be the angle of Δt relative to u_1^B , Figure 2a. Figure 2b depicts the bias as function of θ for different values of $R_{Y \sim U|T}^2$. When Δt is in the null space of B , $\text{PATE}_{\Delta t}$ is identified because the confounder distributions are identical in the two treatment arms, i.e. there is no confounding for this particular contrast. When Δt is colinear with u_1^B the scaled difference in means of u is largest, which implies the largest worst-case bias for the treatment effect, Figure 2c (left). Even when $\text{PATE}_{\Delta t}$ is identified, we emphasize that $\text{PATE}_{t_1,\cdot}$ and $\text{PATE}_{t_2,\cdot}$ are both biased,

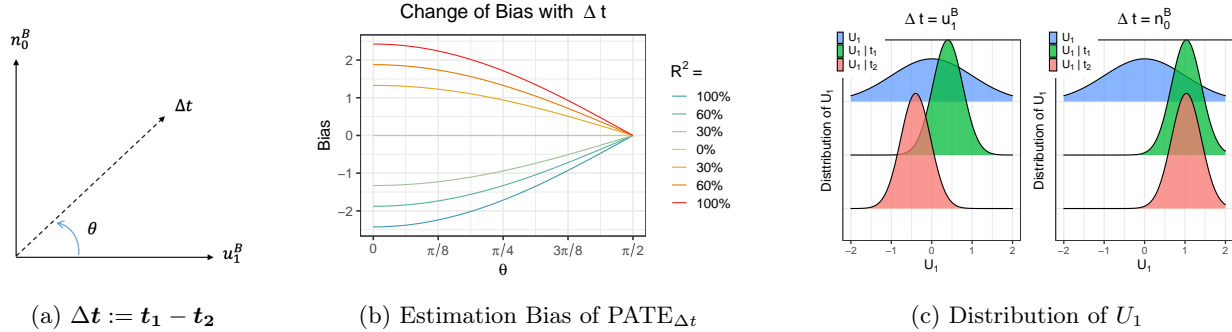


Figure 2: Illustration of Corollary 3.1. (a) We parameterize Δt with θ , the angle between n_0^B , a vector in the null space of B , and u_1^B , the first left singular vector of B . (b) The confounding bias of naive estimates of $\text{PATE}_{\Delta t}$ changes with θ and depends on $R^2_{Y \sim U|T}$. (c) Confounder densities in different populations. The blue, green, red densities denote distributions of U_1 in the observed population, the subpopulation receiving t_1 and the subpopulation receiving treatment t_2 respectively. Observed data estimates of $\text{PATE}_{\Delta t}$ are unbiased when $\Delta t = n_0^B$, since the confounder distributions are the same in two treatment arms. However, observed data estimates of $\text{PATE}_{t_1,\cdot}$ and $\text{PATE}_{t_2,\cdot}$ are biased since in general the superpopulation distribution of the confounder is different.

since the distribution of confounders in the treatment arm differs from the distribution of confounder in the superpopulation, Figure 2c (right). As noted by others, identification of $\text{PATE}_{\Delta t}$ for Δt in the null space of B arises due to bias cancellation in intervention means of the two treatment arms (Grimmer et al., 2020).

Our theory is invariant to rotations of the treatments vector, which means that under model 17-19, we can always make a change of treatment variables so that each confounder affects a distinct single rotated treatment (called “single cause” confounders in Wang and Blei (2018)). Specifically, let $\tilde{T} = RT$ be a rotation of the original treatment variables, so that $\tilde{T} \sim N(0, \Delta + \sigma_{t|u}^2 I_k)$ where Δ is a diagonal positive semi-definite matrix. Then, as before, $\frac{\Delta_i}{\Delta_i + \sigma_{t|u}^2}$ is the fraction of variance in the i th rotated treatment due to confounding and provides a bound on the omitted confounder bias of estimates of PATE for $\Delta \tilde{T} = e_i$. For the $k - m$ contrasts corresponding to the zeros in the diagonal of Δ , there is no confounding for these particular treatment contrasts and thus there is no confounding bias; these correspond to the contrasts in the original space which fall in the null space of B .

5.2 Generalizing the Linear-Gaussian Model

Next, we generalize beyond the setting in which (Y, T, U) is jointly multivariate Gaussian. First, when Y is Gaussian with mean $\mu_{y|t}$ and variance $\sigma_{y|t}^2$, even when T has an arbitrary functional relationship with Y we have that

$$\text{PATE}_{t,\cdot} = (\mu_{y|t} - \mu_y) - \sigma_{y|t} \gamma'(\mu_{u|t} - \mu_u), \quad (35)$$

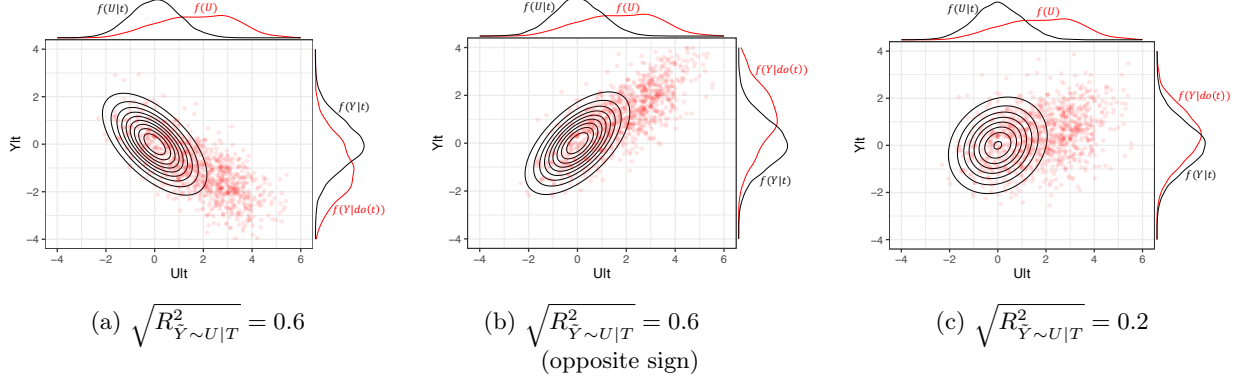


Figure 3: Differences between observed and intervention densities as a function of the fraction of outcome variance explained by a single confounder. The black contours depict the conditional Gaussian copula, $c_\gamma(F_{Y|t}(y), F_{U|t}(u) | t)$ whereas red points represent samples from the joint distribution, $f(y, u | do(t)) \propto f(y | t)c_\gamma(F_{Y|t}(y), F_{U|t}(u) | t)f(u)$. We visualize the shift in the outcome density for different conditional correlations and note that smaller values of $R_{Y \sim U|T}^2$ imply smaller biases in the outcome despite large imbalance in the distribution of U .

where $\mu_u = E[U]$ is the population mean of U . Thus,

$$\text{PATE}_{t_1, t_2} = (\mu_{y|t_1} - \mu_{y|t_2}) - \sigma_{y|t} \gamma' (\mu_{u|t_1} - \mu_{u|t_2}). \quad (36)$$

This leads to the following generalization of Theorem 3.

Theorem 4. *Assume the model 13-15 with Gaussian outcomes. If $\Sigma_{u|t}$ is non-invertible, then Bias_{t_1, t_2} is bounded if and only if $\mu_{u|t_1} - \mu_{u|t_2}$ is in the row space of $\Sigma_{u|t}$. When bounded,*

$$\text{Bias}_{t_1, t_2}^2 \leq \sigma_{y|t}^2 R_{Y \sim U|T}^2 \|(\Sigma_{u|t}^\dagger)^{1/2} (\mu_{u|t_1} - \mu_{u|t_2})\|_2^2, \text{ where } \Sigma_{u|t}^\dagger \text{ is the pseudo-inverse of } \Sigma_{u|t}.$$

Proof: See Appendix.

As before, when bounded, the bias is proportional to the norm of the scaled difference in confounder means in the two treatment arms.

When there exists an m -vector, q , such that $\text{Var}(q'U | t) = 0$, then $\Sigma_{u|t}$ is non-invertible because there exists a projection of the confounders which is point identified. Theorem 4 says that in this case, the ignorance region for the PATE is bounded if and only if $q'(\mu_{u|t_1} - \mu_{u|t_2}) = 0$. In words, if a projection of the confounders can be identified, then the confounding bias is bounded if the identifiable projection of the confounders has the same value in both treatment arms. This result can be viewed in the context of Theorem 7 in Wang and Blei (2018), which assumes consistency and overlap of estimators for the relevant latent confounders for identification.

When the observed outcome distribution is non-Gaussian, we cannot necessarily express PATE_{t_1, t_2} analytically. In particular, for non-Gaussian Y , when $f(u | t_1) \sim f(u | t_2)$ the average treatment effect among the t_1 and t_2 treated units is unconfounded, but the bias of PATE_{t_1, t_2} may be nonzero since $f(u | t) \approx f(u)$. The causal effects, however, can still be calculated using Algorithm 1. Another particularly important non-Gaussian setting we highlight here is when the outcome is binary. Interestingly, unlike the linear case, RR_t , and RR_{t_1, t_2} are non-monotone in the magnitude of γ . We discuss this in more detail in Appendix B.3 and provide simulation results with binary outcomes in Section 7.

6 Calibration and Robustness

Sensitivity analyses consist of two parts: first, the sensitivity model itself, which specifies a set of causal models, indexed by sensitivity parameters; and secondly, exploratory tools for mapping external assumptions to particular causal models in this set. We now turn to discussing the latter in the context of our proposed model.

In the sensitivity analysis literature so far, two exploratory techniques have been particularly popular in single treatment studies: *calibration*, which maps sensitivity parameter values to interpretable observable or hypothetical quantities; and *robustness analysis*, which characterizes the “strength” of confounding necessary to change the conclusion of a study. Here, we show how to adapt these techniques to our sensitivity model in the multi-treatment setting. In addition, we introduce a third class of tools that are particularly well-suited to the multi-treatment setting, which we call *multiple contrast criteria* (MCCs). MCCs specify aggregate properties of the treatment effects for multiple treatment contrasts that are implied by a single causal model, e.g., the L2 norm of PATEs corresponding to contrasts in each individual treatment variable in T . In many multi-treatment settings, assumptions are often expressed in terms of the aggregates—e.g., in genomics, the idea that the effect of most single nucleotide polymorphisms is small—and we show here how these can be used in conjunction with our sensitivity model to characterize candidate causal models that may be of interest in an application.

6.1 Calibration For a Single Contrast

We begin by describing calibration for γ in our sensitivity model when the focus is on a single treatment contrast, between levels $T = t_1$ and $T = t_2$. The goal is to develop heuristics for specifying “reasonable”

values or ranges for γ , e.g., to derive bounds on treatment effects by specifying bounds on the strength or direction of confounding. Following previous work in the single treatment setting, we outline how to calibrate our sensitivity parameter vector γ in terms of a fraction of outcome variance explained by the unobserved confounder. Recall that γ is a vector that parameterizes the residual correlation between the m -dimensional unobserved confounder U and the outcome Y after conditioning on the treatment vector T .

First, we briefly review calibration in single-treatment settings. In latent variable approaches for single treatment sensitivity analysis, the causal effect is identified given two sensitivity parameters: the fraction of outcome variance explained by unobserved confounders, $R_{Y \sim U|T}^2$, and the fraction of treatment variance explained by unobserved confounders, $R_{T \sim U}^2$ (Cinelli and Hazlett, 2019). In a linear model, these two scalar quantities identify the confounding bias (Equation 29). Neither R-squared value is identifiable and thus many authors have proposed strategies for drawing analogies between these values and other observable or hypothetical quantities (Cinelli et al., 2020; Veitch and Zaveri, 2020; Franks et al., 2019).

We borrow this strategy for calibration in our setting, with some modifications. First, in our setting there is no need to calibrate $R_{T \sim U}^2$, because we have restricted ourselves to the case where $f(u | t)$ is identified up to a causal equivalence class. This leaves calibration of the outcome-confounder relationship, which in our setting is more complex because it is parameterized by a vector γ^1 . However, we can reparameterize γ in terms of a direction d and an R-squared for interpretable calibration:

$$\gamma = \sqrt{R_{Y \sim U|T}^2} \Sigma_{u|t}^{-1/2} d, \tag{37}$$

where $d \in \mathbb{S}^{m-1}$ is an m -dimensional unit vector. We discuss strategies for calibrating both the magnitude and direction separately.

Calibrating the magnitude of γ . For Gaussian outcomes, the magnitude of γ is characterized entirely by $R_{Y \sim U|T}^2$, the partial fraction of outcome variance explained by U given T . When $R_{Y \sim U|T}^2 = 0$ there is no unobserved confounding and when $R_{Y \sim U|T}^2 = 1$, all of the observed residual variance in Y is due to confounding factors. In order to calibrate this magnitude, we adopt an idea proposed by Cinelli and Hazlett (2019) for inference with single treatments. In their work, they calibrate $R_{Y \sim U|T}^2$ by comparing it to the partial fraction of variance explained by different observed covariates. We use a closely related strategy that makes use of the presence of multiple treatments rather than observed covariates. Specifically, we compute

¹Unlike the single treatment setting, the confounder-outcome relationship cannot be sufficiently summarized in terms of a scalar $R_{Y \sim U|T}^2$. Each confounder can impact each treatment in different ways.

the fraction of variation in Y that can be explained by a specific treatment (or set of treatments), T_j , after controlling for all other treatments T_{-j} as

$$R_{Y \sim T_j | T_{-j}}^2 := \frac{R_{Y \sim T}^2 - R_{Y \sim T_{-j}}^2}{1 - R_{Y \sim T_{-j}}^2}, \quad (38)$$

When observed covariates are available, we can still analogously compute the partial fraction of variance explained by an observed covariate, $R_{Y \sim X_j | T, X_{-j}}^2$, as done in [Cinelli and Hazlett \(2019\)](#). [Veitch and Zaveri \(2020\)](#) and [Cinelli et al. \(2020\)](#) propose useful graphical summaries for calibration based on these metrics in the single treatment setting.

When the observed outcome is non-Gaussian, we calibrate the “implicit R^2 ”, by considering the explained variance of the latent Gaussian outcome, \tilde{Y} in Equation 14. The implicit R^2 of T for model 13-15 is defined as

$$R_{\tilde{Y} \sim T}^2 = \frac{\text{Var}(E[\tilde{Y}|T])}{\text{Var}(E[\tilde{Y}|T]) + 1}. \quad (39)$$

and the implicit partial R-squared of treatment T_j , $R_{\tilde{Y} \sim T_j | T_{-j}}^2$, is defined analogously to Equation 38. As before, these estimable partial R-squared values can be used to provide a useful comparison for the partial R-squared of potential unobserved confounders, $R_{\tilde{Y} \sim U | T}^2$. For more detail, see [Imbens \(2003\)](#) and [Franks et al. \(2019\)](#) who discuss calibration with implicit R-squared values in logistic regression models.

Choosing the direction of γ . Given a magnitude, we now propose a default method for identifying the direction of γ for a single contrast. The dot product $d' \Sigma_{u|t}^{-1/2} (\mu_{u|t_1} - \mu_{u|t_2})$ corresponds to the projection of the scaled difference in confounder means onto the outcome space. By default, we suggest using the direction which maximizes the squared bias. As shown in Theorem 4, when d is colinear with $\Sigma_{u|t}^{-1/2} (\mu_{u|t_1} - \mu_{u|t_2})$, the confounding bias of the naive estimator for Gaussian outcomes is maximized at

$$|\text{Bias}_{t_1, t_2}| = \sqrt{R_{Y \sim U | T}^2 \sigma_{y|t}} \|\Sigma_{u|t}^{-1/2} (\mu_{u|t_1} - \mu_{u|t_2})\|_2, \quad (40)$$

Choosing the direction of the sensitivity vector in this way provides conservative bounds for each contrast of interest. For non-Gaussian outcomes or alternative estimands, there may not be an analytic solution to the direction which maximizes the bias, but we can still compute the direction via numerical optimization.

6.2 Robustness for Single Contrasts

We now turn to assessing the robustness of conclusions using our sensitivity model, extending work by [Cinelli and Hazlett \(2019\)](#) and [VanderWeele and Ding \(2017\)](#) in the single treatment setting. Specifically, we propose an extension of the robustness value (RV), which characterizes the minimum strength of confounding needed to change the sign of the treatment effect. As in the previous section, the extension is most straightforward when considering the effect of a single treatment contrast, between levels $T = t_1$ and $T = t_2$.

To review briefly, in single treatment settings, Cinelli and Hazlett define the RV as the minimum R -squared needed to reduce the treatment effect to zero, assuming $R_{Y \sim U, T}^2 = R_{T \sim U}^2$. (we return to this assumption below.) A robustness value close to one means the treatment effect maintains the same sign even if nearly all of the observed residual variance in the outcome is due to confounding. On the other hand, a robustness value close to zero means that even weak confounding would change the sign of the point estimate.

In the multi-treatment setting, we can more precisely characterize the robustness of causal effects when $R_{T \sim U}^2$ is identifiable. In particular, we can compute an analogue to the RV without assuming $R_{Y \sim U, T}^2 = R_{T \sim U}^2$, an assumption that, in single treatment settings, can be consequential². With $R_{T \sim U}^2$ known, we define multi-treatment RV can then simply as the minimum value of $R_{Y \sim U|T}^2$ needed to explain away the treatment effect of interest, assuming the direction of the sensitivity vector is chosen to maximize the bias. When the observed outcomes are Gaussian, the robustness value can be computed in closed form:

$$RV_{t_1, t_2} = \frac{(\mu_{y|t_1} - \mu_{y|t_2})^2}{\sigma_{y|t}^2 \|\Sigma_{u|t}^{-1/2} (\mu_{u|t_1} - \mu_{u|t_2})\|^2}, \quad (41)$$

RV metrics for alternative estimands and/or non-Gaussian data can still be computed using the same principle. For example, when the observed outcome is binary, the RV can be computed numerically by solving $RR_{t_1, t_2} = 1$, which corresponds to the minimum strength of confounding needed for the observed risk ratio (RR) to equal to one. This robustness value is analogous to the ‘‘E-value’’ proposed by [VanderWeele and Ding \(2017\)](#).

In our setting, we can also make stronger statements about robustness than in the single treatment setting: under the latent variable model, it is possible to declare an effect robust to *any* level of confounding.

²In single treatment settings, when $R_{Y \sim U|T}^2 > R_{T \sim U}^2$, the single-treatment RV will be too conservative. Conversely, when $R_{Y \sim U|T}^2 < R_{T \sim U}^2$ the single-treatment RV will overestimate the robustness of the effect.

In particular, when the latent variable model implies $R_{T \sim U}^2 < 1$ (i.e., we have confounder overlap), then even when $R_{Y \sim U|T}^2 = 1$, the ignorance region is bounded (Theorem 4). When this ignorance region excludes zero, we declare the effect “robust”. This operation is consistent with the result in Miao et al. (2018), showing that hypotheses of zero effect can be tested in this setting, even if the treatment effect cannot be identified.

6.3 Multiple Contrast Criteria

In addition to exploratory tools used with single-treatment sensitivity analysis, the multi-treatment setting presents opportunities for exploring sensitivity models in new ways. Here, we propose one such approach using multiple contrast criteria, or MCCs. As opposed to the approaches we have discussed so far, which consider treatment contrasts in isolation, MCCs characterize a choice of sensitivity vector γ by concurrently considering its implications for multiple treatment contrasts in aggregate. Thus, while the sensitivity vector γ that gives the worst-case bias may differ across individual contrasts, an MCC can be used to select a single γ that has implications for many simultaneous treatment effects.

Formally, for a set of treatment contrasts $\mathcal{T}^2 = \{(t_1, t_2)_k\}_{k=1}^K$, and a candidate sensitivity vector γ , let $\mathbf{PATE}_{\mathcal{T}^2}(\gamma)$ be the vector of PATEs implied by the causal model indexed by γ . An MCC is a scalar summary of this treatment effect vector, which we write as $\omega(\mathbf{PATE}_{\mathcal{T}^2}(\gamma))$. An MCC is specified by the set of contrasts \mathcal{T}^2 and the summary function ω , both of which can be chosen to meet the needs of a given analysis.

MCCs can be used in many ways, but here we consider how they can be used to search for the causal model that yields the minimum norm treatment effect vector, subject to assumptions 1-5 and a confounding limit \mathcal{R}^2 . Specifically, we take ω to be an L_p norm for some p , and consider sensitivity vectors γ_* that satisfy:

$$\gamma_* = \underset{\tilde{\gamma}}{\operatorname{argmin}} \omega(\mathbf{PATE}_{\mathcal{T}^2}(\tilde{\gamma})) \text{ subject to } R_{Y \sim U|T}^2(\tilde{\gamma}) \leq \mathcal{R}^2 \quad (42)$$

where $R_{Y \sim U|T, X}^2(\tilde{\gamma}) = \frac{\tilde{\gamma}' \Sigma_{u|t} \tilde{\gamma}}{\sigma_{y|t}^2}$ is the partial fraction of outcome variance explained by confounding for sensitivity vector $\tilde{\gamma}$. Causal models selected in this way are often highly interpretable, in terms of either “worst case” effect sizes or established prior knowledge. For example, we can chose ω to be the L_∞ norm, so that γ_* is the sensitivity vector that minimizes the maximum absolute effect across contrasts. Alternatively, we could choose ω to be the L_1 or L_2 norm of the treatment effects to find models that imply small “typical” effect sizes. We demonstrate how this minimization approach can be used to express prior knowledge about

small effects in simulated data in Section 7.2, and how it can be used to evaluate robustness on a real data set in Section 8.

7 Simulation Studies

In this Section, we demonstrate our sensitivity analysis workflow in several numerical simulations. The goal of these simulations is twofold: first, to demonstrate some of the operating characteristics of the approach in settings that are more realistic than the linear Gaussian settings we characterized analytically; and secondly, to show how exploratory tools like calibration, robustness analysis, and MCCs can be used to draw conclusions and choose interesting candidate models.

We consider two broad simulation settings. In the first setting, we construct simulations with non-linear responses to treatment to show how the ignorance regions returned by our method can vary in different scenarios. In the second setting, we construct a simulation that mimics the structure of a Genome Wide Association Study (GWAS). Here, we examine the behavior of our method when a popular approximate latent variable method—the Variational Auto Encoder (VAE)—is used to estimate the effects of latent confounders, and demonstrate how MCCs can be useful tools for using prior information to choose potentially useful causal models from the set that is compatible with the observed data. In both subsections, we simulate data from the following generating process:

$$U := \epsilon_u, \quad \epsilon_u \sim N_m(0, I_m), \tag{43}$$

$$\tilde{T} := BU + \epsilon_{t|u}, \quad \epsilon_{t|u} \sim N_k(0, \sigma_{t|u}^2 I_k), \tag{44}$$

$$T := h_T(\tilde{T}), \tag{45}$$

$$\tilde{Y} := g(T) + \gamma'U + \epsilon_{y|t,u}, \quad \epsilon_{y|t,u} \sim N(0, \sigma_{y|t,u}^2), \tag{46}$$

$$Y := h_{Y|T}(\tilde{Y}), \tag{47}$$

The functions h_Y and h_T are chosen according to be either the identity for Gaussian data, or an indicator function for binary data.

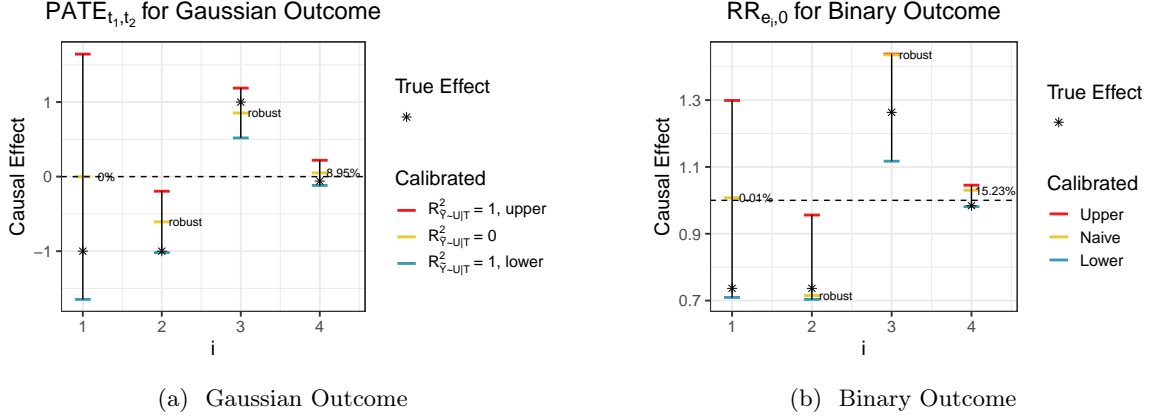


Figure 4: Estimated ignorance region for e_i in case when \tilde{Y} is nonlinear in T . (a) $R_{\tilde{Y} \sim U|T}^2 = 0$ denotes the treatment effects estimated based on the observed data only, i.e., under the assumption of no confoundedness. $R_{\tilde{Y} \sim U|T}^2 = 1$ and $R_{\tilde{Y} \sim U|T}^2 = 1$ correspond to the case when all residual variation in Y is due to the confounding, respectively denoting the upper and lower bounds of the ignorance region. (b) In the binary setting, even though the estimand is a non-linear function of the latent Gaussian outcome, the width of the ignorance region and general robustness pattern is largely consistent with the implications of Corollary 3.1.

7.1 Example with Non-Linear Response Functions

We start by exploring variation in the size of ignorance regions for different contrasts in a simple simulated example with four treatments where the outcome is a nonlinear function of these treatments. We consider two cases: first, a case where Y is Gaussian with $h_Y(\tilde{Y}) = \tilde{Y}$; and secondly, a case where Y is binary with $h_Y(\tilde{Y}) = I_{\tilde{Y} > 0}$. We aim to estimate the $\text{PATE}_{e_i, 0}$ for Gaussian outcome and $\text{RR}_{e_i, 0}$ for binary outcome, where e_i denotes the i th canonical vector, i.e. the vector with a 1 in the i -th coordinate and 0's elsewhere.

In both examples, we generate the data with a 1-dimensional latent confounder ($m = 1$), $k = 4$ treatments, $B = [2, 0.5, -0.4, 0.2]$, $\sigma_{t|u}^2 = 1$, $\gamma = 2.8$, $\sigma_{y|t, u}^2 = 1$, $h_T(\tilde{T}) = \tilde{T}$ and

$$g(T) = 3T_1 - T_2 + T_3 I_{T_3 > 0} + 0.7T_3 I_{T_3 \leq 0} - 0.06T_4 - 4T_1^2.$$

Based on the choice of g , contrasts along the j th dimension of T have effects of widely varying magnitude. Based on our choice for B , the worst-case confounding bias also varies significantly across contrasts. For example, the effect of confounding is larger when estimating the treatment of T_1 , since the first entry of B has the largest magnitude, meaning T_1 is the feature most correlated with U . In order to demonstrate this in simulation, we first apply probabilistic PCA (PPCA) to estimate the distribution $f(u | t)$, and then model $f(y | t)$ using Bayesian Additive Regression Tree (BART) with R package BART (McCulloch et al., 2018).

For Gaussian outcomes, the width of the ignorance regions are larger for the treatments most correlated with confounders as characterized Theorem 4 (see Figure 4). Since B is a vector, the width of the ignorance region of PATE_{t_1, t_2} can be examined by looking at the dot product between B and the treatment contrasts. The larger the dot product, the wider the ignorance region. As expected, the ignorance region of the treatment effect is widest when $t_1 = e_1$ ($\text{RV} \approx 0\%$) and narrowest when $t_1 = e_4$, since $B'e_1$ has the largest magnitude while $B'e_4$ has the smallest. Despite the fact that $t_1 = e_4$ has the smallest ignorance region, it is not robust to confounding because the naive effect is already close to zero ($\text{RV} = 9\%$). For the second and third treatment contrasts, estimates are robust to confounders, as their entire ignorance regions exclude 0.

For the simulation with binary outcomes, we compute ignorance regions for the risk ratio. Although we do not have a theoretical result about the ignorance regions of the risk ratio, the general trends in the size of the ignorance region and the robustness of effects are comparable to the Gaussian. Most notably, the treatments with the largest ignorance regions are still those which are most correlated with the confounder. On the other hand, because the outcome is non-linear in U , the naive estimate is not at the center of the ignorance region (Figure 4b). In fact, the ignorance region is also non-monotone in $R_{\tilde{Y} \sim U|T}^2$ because the variance of the intervention distribution also depends on γ . In this case, one of the endpoints of the ignorance region corresponds to $R_{\tilde{Y} \sim U|T}^2 = 1$ but the other does not. We compute the endpoints of the ignorance region numerically (see Appendix B.3 for more details).

7.2 Example with Simulated Genome Wide Association Study

We now explore a slightly more complex setting motivated by applications in biology, particularly in genome wide association studies (GWAS). GWAS investigate the association between hundreds or thousands of genetic features (i.e., single nucleotide polymorphisms, or SNPs) and observable traits (i.e., phenotypes), such as disease status. Here, we construct a simulated GWAS to demonstrate two properties of our sensitivity analysis method. First, we show that flexible latent variable models can be plugged into our sensitivity model. Secondly, we demonstrate how minimizing multiple contrast criteria (MCC) can be used to select interesting candidate models that conform to broad hypotheses about the nature of genetic effects.

Despite having “association” in the name, GWAS is a particularly interesting application area for multi-treatment causal inference. In practice, measures of association in GWAS are often adjusted to afford a causal interpretation in which conclusions speak to how a phenotype would change if the genome were intervened upon. For example, most analyses adjust for “population structure”, which correspond to broad genetic

patterns induced by population dynamics that are often confounded with geography, ancestry, environment, and other lifestyle factors (Price et al., 2006; Song et al., 2015). Wang and Blei (2018) cite this literature as motivation for their work.

In this simulation, we generate data with high-dimensional binary treatments (SNPs), and set the true causal effects to be mostly small, with a small fraction of treatments having effects of larger magnitudes. The simulation is then designed so that unobserved confounding biases estimates for each of these treatment effects, obscuring the difference between large and small effects. To generate data, we follow the template in Equations 43–47. We generate data with $m = 3$ latent confounders and $k = 500$ treatments, $T \in \{0, 1\}^k$, where $T_j = 1$ if the the j th site shows a deviation from the baseline sequence (i.e., the presence of at least one minor allele). We set the response function $g(T) = \tau'T$ to be linear in the treatments (a common assumption in GWAS), and set the outcome Y to be Gaussian by setting $h_Y(\tilde{Y}) = \tilde{Y}$. We focus on estimating

$$\frac{1}{n} \sum_{i=1}^n PATE_{t_i^j, t_i^{-j}} \text{ for all } j = 1, \dots, k, \quad (48)$$

where t_i^j and t_i^{-j} correspond to the i^{th} observed treatment vector with the j^{th} SNP set to be 1 and 0 respectively. Note that since $g(T)$ is linear in T , $\frac{1}{n} \sum_{i=1}^n PATE_{t_i^j, t_i^{-j}} = \tau_j$, the j^{th} element of τ . We generate τ from a two component mixture with 90% of the coefficients from a Uniform($-0.1, 0.1$) (small effects) and 10% from a Uniform($-2, 2$) (large effects). We assume that there are $m = 3$ latent confounders.

We consider a model for the observed data with two components, paying special attention to the latent confounder model. In particular, we model the conditional distribution of confounders given treatment $f(u | t)$ using a variational autoencoder (VAE), which is a popular, flexible neural network–based approximate latent variable model. This model is particularly appropriate because it yields an approximate Gaussian conditional distribution $f(u | t)$, even for discrete T as we have here. (We discuss latent confounder inference with VAEs in more detail in Appendix B.2.) We fit the observed outcome model $f(y | t)$ using a simple linear regression, ignoring confounding, which corresponds to the setting in which $R_{Y \sim U|T}^2 = 0$.

Worst-Case Ignorance Regions. With this simulation setup, we first examine whether the ignorance regions contain to the true causal effects. Importantly, because the VAE is an approximate latent variable model, and we are currently ignoring estimation uncertainty, it is not immediate that the ignorance regions should be valid. We find that, even using our plug-in approach, the worst case ignorance regions cover 498 out of 500 of the true treatment effects. In all cases, the worst case bounds communicate substantial

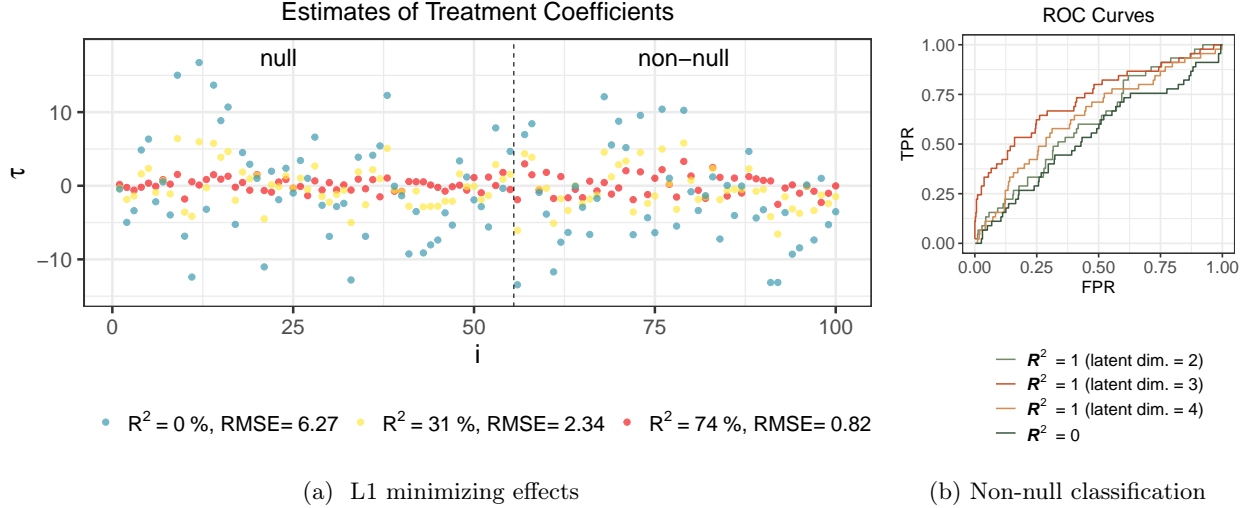


Figure 5: Causal inference with 500 binary treatments with $k = 3$ latent confounders. Naive estimates of the null and non-null effects are overdispersed due to confounding. (a) Minimum L1-norm treatment effects are shown for fifty randomly chosen small effects (“null” contrasts) and all large effects (“non-null” contrasts) for three different limits on the magnitude of confounding, $\mathcal{R}^2 \in \{0, 0.3, 1.0\}$. When $\mathcal{R}^2 = 1$, there overall L1 minimizer of the treatment effects is achieved for the sensitivity vector which explains $R^2_{Y \sim U|T} = 74\%$ of the residual outcome variance. (b) We construct a simple non-null classifier from minimum L1 treatment effects with $\mathcal{R}^2 = 1$ and naive effects ($\mathcal{R}^2 = 0$). The blue curve represents the ROC curves from the naive estimates and the green, yellow and red curves represents the L1 minimizer of the treatment effect estimates for inferred confounder models with dimensions $\hat{k} \in \{2, 3, 4\}$. The area under the curve (AUC) for the naive estimates is 0.54, whereas the AUC for the L1-minimized estimates are 0.61 ($\hat{k} = 2$), 0.73 ($\hat{k} = 3$) and 0.64 ($\hat{k} = 4$).

fundamental uncertainty about the true treatment effects (See Appendix Figure 8).

Finding Candidate Models with MCCs. Investigators often have strong hypotheses about the aggregate properties of SNP treatment effects. For example, while some phenotypes can be predominantly explained by only a small number of SNPs, other phenotypes may be more plausibly described by the omnigenic hypothesis, which suggests that some observable effects must be explained by the sum of many small effects across many SNPs (Boyle et al., 2017). Here, we show that some of these aggregate hypotheses can be formalized in terms of MCCs, and in these cases, the MCC minimization procedure from Section 6.3 can be used to find useful candidate causal models that align with these hypothesis while being fully consistent with the observed data.

To motivate candidate model selection, we consider the use case of estimating effect sizes from a single coherent model, under the hypothesis that the median effect size is small. Specifically, we formalize this hypothesis by defining a MCC $\omega(\mathbf{PATE}_{\mathcal{T}^2}(\gamma))$ to be the L_1 norm of the effects of each contrast $\mathcal{T}^2 =$

$\{(t_i^j, t_i^{-j}) : i \in (1, \dots, n)\}$ for all treatments $j = 1, \dots, k$. We then select the model that minimizes this criterion by selecting γ subject to different allowed levels of confounding $R_{Y \sim U|T}^2$.

In Figure 5a, we plot the the resulting coefficients estimates for three values of \mathcal{R}^2 : 0 (naive effects), 0.3 and 1. Because the true effects are much smaller in magnitude than the naïve effects, the RMSE of the estimates decreases as we increase $R_{Y \sim U|T}^2$, although all effects are equally compatible with the observed data. In this simulation, the L1 norm of naive estimates is approximately 2525 and the norm of the true effects is drastically smaller at approximately 75.

Models selected using this MCC minimization procedure are also useful for the coarser goal of separating small and large effects. From the naive regression, the coefficients are overdispersed to the true causal effects and the true small coefficients are practically indistinguishable from true large coefficients. Meanwhile, models chosen with the MCC minimization procedure provide more useful signal. To formalize this, we consider a classifier that separates large and small effects using the magnitude of the inferred coefficients as the classification score. In Figure 5 we plot the receiver operating characteristic (ROC) curves for the classifiers based on the naive estimates as well as the overall $L1$ minimizer of the treatment effects ($\mathcal{R}^2 = 1$, i.e. no limit on the value $R_{Y \sim U|T}^2$).

Importantly, the difference in conditional confounder means, $\mu_{u|t_i^j} - \mu_{u|t_i^{-j}}$, varies between non-null and null contrasts. This leads to a larger reduction in the relative magnitude of the null effects for models chosen through MCC minimization, accentuating the differences between large and small treatment effects (See Appendix Figure 9). For models selected by MCC minimization, the area under the ROC curve (AUC) increases from 0.54 (almost no ability to distinguish small and large treatments) to 0.72 ($\hat{k} = 3$, red curve). The selected model achieves nearly 25% true positive rate without accruing any false positives. Naturally, the classifier performance is the best when we fit a latent variable model with the correct number of latent factors, although the classifier based on latent variable models of dimensions $\hat{k} = 2$ and $\hat{k} = 4$ still outperform classification from naive effects. In the Discussion, we note how this approach relates to, and complements recent identification results for a similar setting in Miao et al. (2020).

8 A Reanalysis of the Actor Case Study

In this section, we compare our approach to other recent analyses of the TMDB 5000 Movie Dataset (Kaggle, 2017) which was analyzed extensively by Wang and Blei (2018) and Grimmer et al. (2020). The dataset

consists of 5000 movies and their corresponding revenue, budget, genre and the identities of the lead cast members. Following Wang and Blei, we focus on estimating the causal effect of an actor’s presence on the movie’s log revenue. We let Y denote the log revenue and $T_i = (T_{i1}, \dots, T_{ik})$ encode the movie cast, where the binary random variable $T_{ij} \in \{0, 1\}$ indicates whether actor j appeared in the movie i and $T_i \in \mathcal{T} = \{T_1, \dots, T_n\}$. We also let \mathcal{T}^j denote the set of all movies T_i for which $T_{ij} = 1$. We define the estimand of interest, η_j , as the the total log revenue contributed by actor j :

$$\eta_j := \sum_{t_i \in \mathcal{T}^j} \text{PATE}_{t_i, t_i^j} \quad (49)$$

where t_i^j corresponds to the observed treatment vector for movie i excluding actor j . This estimand is a non-parametric generalization of the regression coefficient τ_j , which was targeted in the analysis in Wang and Blei (2018). Specifically, under the assumption that log-revenue is linear in the cast indicators, η_j reduces to $n_j \tau_j$, the effect of actor j scaled by the number of movies they appeared in, where τ_j are the regression coefficients for actor j . Our estimand is well-defined without this linearity assumption.

We regress the log revenue on cast indicators to estimate actor effects, τ_j^{naive} , under an assumption of no unobserved confounding. In order to demonstrate the applicability of our sensitivity analysis, we explicitly induce unobserved confounding by excluding observed confounders. We validate our analysis, by comparing calibrated effect estimates when the confounders are excluded to estimates when the confounder is included. Most importantly we exclude the movie’s budget which we estimate to be the largest known source of confounding (computed using Equation 38, see Appendix Figure 10a)³.

For simplicity, we model the observed outcome distribution with a linear regression, although other more flexible outcome models (e.g. BART) can also be used. As in the previous Section, we use a VAE to infer a Gaussian conditional confounder distribution, $f(u | t) \sim N(\mu_{u|t}, \Sigma_{u|t})$ (See Appendix, Section B.2).

Results. Since our focus is on confounding not estimation, in order to limit the influence of estimation uncertainty we subset the data to the $k = 327$ actors who participated in at least twenty movies. This reduces the total number of movies to 2439. We fit the VAE to the treatments and use cross-validation to identify the appropriate latent confounder dimension, which we inferred to be $\hat{m} = 20$ (See Appendix Figure 10b). We then plot the worst-case ignorance region for the causal effect on log revenue as a function of $R_{Y \sim U|T}^2$ for the 46 actors with significant regression coefficients in the naive regression (Figure 6, top).

³For illustrative purposes, we can assume that the budget is pre-treatment, meaning that the budget is decided prior to selecting the cast, which may be a dubious assumption in actuality.

Eight actors in the observed data regression have significantly negative coefficients, whereas 38 actors have significant positive coefficients. However, the worst-case ignorance regions for each actor are all very wide and include zero, which suggests that none of the effects are robust to confounding. In Table 1 of the Appendix we include robustness values for these actors. Leonardo DiCaprio has the largest robustness value at 36%, with the majority of the other actors well below 20%. For reference, the log budget, which was explicitly excluded from our causal analysis, explains about 30% of the variance in log revenue (Appendix Figure 10a). In other words, none of the causal effects are robust at a level which matches the variance explained by the most important excluded confounder.

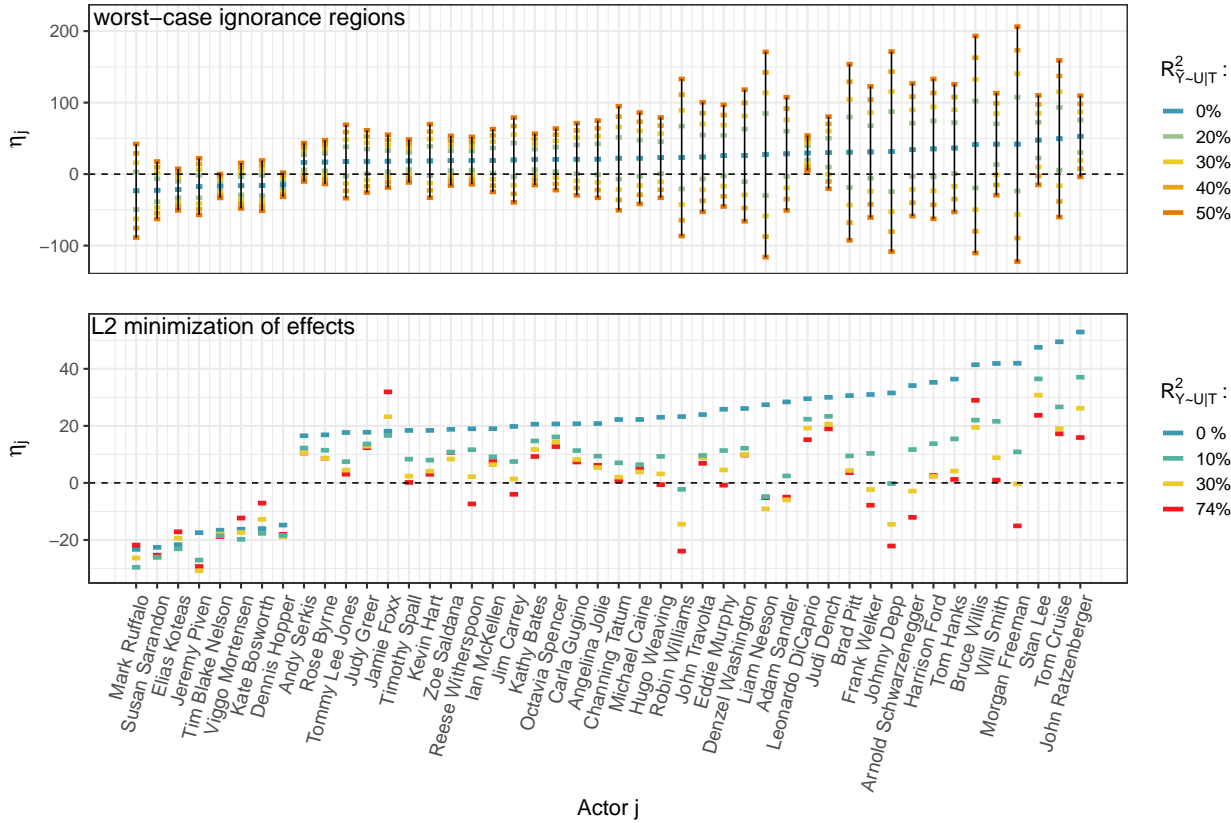


Figure 6: Estimated total log revenue contributed by a given actor. Top: worst-case ignorance region for each actor on a case by case basis. The blue points correspond to $R^2_{Y \sim U|T} = 0$, i.e. the naive estimates. Robustness values can be found in Appendix Table 1. Bottom: Treatment effects for candidate models chosen with the L2 minimizing multiple contrast criterion (MCC). The color correspond to \mathcal{R}^2 , the limit on the fraction of outcome variance explained by confounding.

The worst case ignorance regions depicted in top panel of Figure 6 correspond to a different choice of γ for each actor. We can also explore the robustness of causal effects under a single model by applying an appropriate MCC. Specifically, we search for a “worst case” candidate model by finding the sensitivity

vector, γ_* , that implies the smallest L2 norm of the regression coefficients, τ . In this conservative model, the minimum L2 norm of the treatment coefficients is 4.4, down from 7.6 for the naive coefficients. In addition, 40 out of 46 actors have coefficients that are smaller in magnitude than the magnitudes of the naive coefficients (Figure 6, bottom). For this candidate model, it turns out that $\gamma'_*E[U|T = t]$ is significantly correlated, albeit weakly, with budget (Spearman’s rank correlation = 0.2, p-value < $2e-16$). Thus, the conservative model correctly attributes part of the outcome variation induced by the known excluded confounder to unobserved confounding.

9 Discussion

In this paper, we introduced a framework for sensitivity analysis with multiple treatments which provides further context to the growing literature on the challenges of inference in this setting. Unlike previous work, we emphasize the importance of carefully defined estimands and show that bounds on the magnitude of confounding bias depend on the particular estimands of interest. Our work also provides a practical solution to characterizing and calibrating the robustness of causal effects across multiple treatments in the presence of unobserved confounding. Code to replicate all analyses is available (Zheng, 2021b) and an R package implementing our methodology is also available and in active development (Zheng, 2021a).

There are several interesting generalizations of our proposed approach, many of which center on assumptions about the copula. For example, in many contexts we may be interested in accounting for potential treatment-confounder interactions, in which case the copula, $c(F_{Y|t}(y), F_{U|t}(u) \mid T = t)$, will vary with t . Likewise, as noted, our approach can be applied with non-Gaussian copulas and alternative latent variable models (e.g latent class models), but calibration and model-specification remains a challenge.

Generalizations based on joint inference of the treatment and outcome models should also be explored. In practice, causal effect estimates may be overdispersed about the true effects due to a combination of sampling variance and unobserved confounding. Joint inference might be especially useful for accounting for both estimation uncertainty and uncertainty due to unobserved confounding. This is particularly important for the multiple contrast criteria which, as described, does not incorporate parameter uncertainty into the objective function. A simple solution in a Bayesian analysis would be to characterize posterior uncertainty by applying the criteria to each MCMC sample of the naive causal effect estimates. A more thorough exploration of the interplay between shrinkage estimation (in the classical sense) and MCC shrinkage to

adjust for confounding bias under the “small effects” hypothesis would be interesting to explore in this context.

Finally, we note that there are many promising directions for incorporating additional constraints into the calibration criteria. One direction of particular interest is to follow the line of research on negative control exposures (NCE) (Shi et al., 2020). A set of NCEs would be subset of causes that were known a priori to have zero (or bounded) causal effect on the outcome, for example genes in a GWAS which were known to be causally unrelated to a particular phenotype. Incorporating these assumptions would further constrain the ignorance regions for particular causal contrasts of interest. These strategies are closely related to the multivariate calibration procedure that we propose. For example, Miao et al. (2020) describe a procedure for identifying the treatment effects when over half of the treatments are assumed to have no causal effect on the outcome. In Equation 42, this would be analogous to the case in which m is the L_0 norm, the number of non-zero effects. It is also worth further exploring the relationship between inference with multiple treatments and inference with multiple outcomes. Additional structure in the correlation between outcomes could further constrain the causal ignorance regions, under the right set of assumptions. As with NCE’s, negative control outcomes (NCOs) could be applied to calibrate the sensitivity analysis. We leave this to future work.

References

- Bica, I., A. M. Alaa, C. Lambert, and M. van der Schaar (2020). From real-world patient data to individualized treatment effects using machine learning: Current and future methods to address underlying challenges. *Clinical Pharmacology & Therapeutics*.
- Boyle, E. A., Y. I. Li, and J. K. Pritchard (2017). An expanded view of complex traits: from polygenic to omnigenic. *Cell* 169(7), 1177–1186.
- Cinelli, C., J. Ferwerda, and C. Hazlett (2020). sensemakr: Sensitivity analysis tools for ols in r and stata. *Submitted to the Journal of Statistical Software*.
- Cinelli, C. and C. Hazlett (2019, 12). Making sense of sensitivity: extending omitted variable bias. *Journal of the Royal Statistical Society Series B (Statistical Methodology)*.
- Cinelli, C., D. Kumor, B. Chen, J. Pearl, and E. Bareinboim (2019). Sensitivity analysis of linear structural causal models. In *ICML*.
- Cornfield, J., W. Haenszel, E. C. Hammond, A. M. Lilienfeld, M. B. Shimkin, and E. L. Wynder (1959). Smoking and lung cancer: recent evidence and a discussion of some questions. *J. Nat. Cancer Inst* 22, 173–203.
- D’Amour, A. (2019a). Comment: Reflections on the deconfounder. *Journal of the American Statistical Association* 114(528), 1597–1601.
- D’Amour, A. (2019b). On multi-cause approaches to causal inference with unobserved confounding: Two cautionary failure cases and a promising alternative. In *The 22nd International Conference on Artificial Intelligence and Statistics*, pp. 3478–3486.

- Daniels, M. J. and J. W. Hogan (2008). *Missing data in longitudinal studies: Strategies for Bayesian modeling and sensitivity analysis*. CRC Press.
- Dorie, V., M. Harada, N. B. Carnegie, and J. Hill (2016). A flexible, interpretable framework for assessing sensitivity to unmeasured confounding. *Statistics in Medicine* 35(20), 3453–3470.
- Everett, B. (2013). *An introduction to latent variable models*. Springer Science & Business Media.
- Franks, A., A. D’Amour, and A. Feller (2019). Flexible sensitivity analysis for observational studies without observable implications. *Journal of the American Statistical Association* (just-accepted), 1–38.
- Gastwirth, J. L., A. M. Krieger, and P. R. Rosenbaum (1998). Dual and simultaneous sensitivity analysis for matched pairs. *Biometrika* 85(4), 907–920.
- Gavish, M. and D. L. Donoho (2014). The optimal hard threshold for singular values is $4/\sqrt{3}$. *Information Theory, IEEE Transactions on* 60(8), 5040–5053.
- Ghosh, P., M. S. M. Sajjadi, A. Vergari, M. Black, and B. Scholkopf (2020). From variational to deterministic autoencoders. In *International Conference on Learning Representations*.
- Gopalan, P., J. M. Hofman, and D. M. Blei (2013). Scalable recommendation with poisson factorization. *arXiv preprint arXiv:1311.1704*.
- Greenland, S. (1996). Basic methods for sensitivity analysis of biases. *International journal of epidemiology* 25(6), 1107–1116.
- Grimmer, J., D. Knox, and B. M. Stewart (2020). Naive regression requires weaker assumptions than factor models to adjust for multiple cause confounding. *arXiv preprint arXiv:2007.12702*.
- Gustafson, P., L. C. McCandless, et al. (2018). When is a sensitivity parameter exactly that? *Statistical Science* 33(1), 86–95.
- Hao, W., M. Song, and J. D. Storey (2015). Probabilistic models of genetic variation in structured populations applied to global human studies. *Bioinformatics* 32(5), 713–721.
- Horn, R. (1985). *Matrix analysis*. Cambridge Cambridge University Press.
- Imbens, G. W. (2003). Sensitivity to exogeneity assumptions in program evaluation. *American Economic Review* 93(2), 126–132.
- Kaggle (2017, Sep). Tmdb 5000 movie dataset. data retrieved from Kaggle, <https://www.kaggle.com/tmdb/tmdb-movie-metadata>.
- Kong, D., S. Yang, and L. Wang (2019). Multi-cause causal inference with unmeasured confounding and binary outcome. *arXiv preprint arXiv:1907.13323*.
- Lechner, M. (1999, December). Identification and Estimation of Causal Effects of Multiple Treatments Under the Conditional Independence Assumption. IZA Discussion Papers 91, Institute of Labor Economics (IZA).
- Lopez, M. J., R. Gutman, et al. (2017). Estimation of causal effects with multiple treatments: a review and new ideas. *Statistical Science* 32(3), 432–454.
- Lopez, R., P. Boyeau, N. Yosef, M. I. Jordan, and J. Regier (2020). Decision-making with auto-encoding variational bayes. *arXiv preprint arXiv:2002.07217*.
- Louizos, C., U. Shalit, J. M. Mooij, D. Sontag, R. Zemel, and M. Welling (2017). Causal effect inference with deep latent-variable models. In *Advances in Neural Information Processing Systems*, pp. 6446–6456.
- Mardia, K. V., J. T. Kent, and J. M. Bibby (1980). *Multivariate analysis*. Academic press.

- McCulloch, R., R. Sparapani, R. Gramacy, C. Spanbauer, and M. Pratola (2018). *BART: Bayesian Additive Regression Trees*. R package version 1.9.
- Miao, W., Z. Geng, and E. J. Tchetgen Tchetgen (2018). Identifying causal effects with proxy variables of an unmeasured confounder. *Biometrika* 105(4), 987–993.
- Miao, W., W. Hu, E. L. Ogburn, and X. Zhou (2020). Identifying effects of multiple treatments in the presence of unmeasured confounding.
- Minka, T. P. (2001). Automatic choice of dimensionality for pca. In *Advances in neural information processing systems*, pp. 598–604.
- Nelsen, R. B. (2007). *An introduction to copulas*. Springer Science & Business Media.
- Ogburn, E. L., I. Shpitser, and E. J. T. Tchetgen (2019). Comment on “blessings of multiple causes”. *Journal of the American Statistical Association* 114(528), 1611–1615.
- Ogburn, E. L., I. Shpitser, and E. J. T. Tchetgen (2020). Counterexamples to "the blessings of multiple causes" by wang and blei. *arXiv preprint arXiv:2001.06555*.
- Pearl, J. (2009). *Causality*. Cambridge university press.
- Price, A. L., N. J. Patterson, R. M. Plenge, M. E. Weinblatt, N. A. Shadick, and D. Reich (2006). Principal components analysis corrects for stratification in genome-wide association studies. *Nature genetics* 38(8), 904–909.
- Pu, Y., Z. Gan, R. Henao, X. Yuan, C. Li, A. Stevens, and L. Carin (2016). Variational autoencoder for deep learning of images, labels and captions. In *Advances in neural information processing systems*, pp. 2352–2360.
- Robins, J. M. (1997). Non-response models for the analysis of non-monotone non-ignorable missing data. *Statistics in Medicine* 16(1), 21–37.
- Robins, J. M., A. Rotnitzky, and D. O. Scharfstein (2000). Sensitivity analysis for selection bias and unmeasured confounding in missing data and causal inference models. In *Statistical models in epidemiology, the environment, and clinical trials*, pp. 1–94. Springer.
- Rosenbaum, P. R. and D. B. Rubin (1983). Assessing sensitivity to an unobserved binary covariate in an observational study with binary outcome. *Journal of the Royal Statistical Society. Series B (Methodological)*, 212–218.
- Rubin, D. B. (1980). Comment. *Journal of the American Statistical Association* 75(371), 591–593.
- Shi, X., W. Miao, and E. T. Tchetgen (2020). A selective review of negative control methods in epidemiology. *arXiv preprint arXiv:2009.05641*.
- Song, M., W. Hao, and J. D. Storey (2015). Testing for genetic associations in arbitrarily structured populations. *Nature genetics* 47(5), 550–554.
- Tipping, M. E. and C. M. Bishop (1999). Probabilistic principal component analysis. *Journal of the Royal Statistical Society: Series B (Statistical Methodology)* 61(3), 611–622.
- VanderWeele, T. J. and O. A. Arah (2011). Bias formulas for sensitivity analysis of unmeasured confounding for general outcomes, treatments, and confounders. *Epidemiology*, 42–52.
- VanderWeele, T. J. and P. Ding (2017, July). Sensitivity analysis in observational research: Introducing the e-value. *Annals of Internal Medicine* 167(4), 268.

- VanderWeele, T. J., B. Mukherjee, and J. Chen (2012). Sensitivity analysis for interactions under unmeasured confounding. *Statistics in medicine* 31(22), 2552–2564.
- VanderWeele, T. J. and I. Shpitser (2013). On the definition of a confounder. *Annals of statistics* 41(1), 196.
- Vansteelandt, S., E. Goetghebeur, M. G. Kenward, and G. Molenberghs (2006). Ignorance and uncertainty regions as inferential tools in a sensitivity analysis. *Statistica Sinica* 16(3), 953–979.
- Veitch, V. and A. Zaveri (2020). Sense and sensitivity analysis: Simple post-hoc analysis of bias due to unobserved confounding. *arXiv preprint arXiv:2003.01747*.
- Wang, Y. and D. M. Blei (2018, May). The Blessings of Multiple Causes. *arXiv e-prints*, arXiv:1805.06826.
- Zhang, B. and E. J. T. Tchetgen (2019). A semiparametric approach to model-based sensitivity analysis in observational studies. *arXiv preprint arXiv:1910.14130*.
- Zhang, L., Y. Wang, A. Ostropolets, J. J. Mulgrave, D. M. Blei, and G. Hripcsak (2019). The medical deconfounder: Assessing treatment effects with electronic health records. *arXiv preprint arXiv:1904.02098*.
- Zheng, J. (2021a). Copsens: Copula-based sensitivity analysis method for unobserved confounding in multi-treatment inference. <https://github.com/JiajingZ/CopSens>.
- Zheng, J. (2021b). Replication code for “copula-based sensitivity analysis for observational multi-treatment causal inference”. <https://github.com/JiajingZ/CopulaSensitivity>.

A Theory

A.1 General Contrast Estimation Algorithm

Algorithm 2 Marginal Contrast Estimation for Arbitrary Copulas

```

1: function COMPUTEMEAN( $t, \psi$ )
2:   for  $k = 1, 2, \dots, M$  do
3:     Sample  $y_k$  from  $f(y | t)$ 
4:     for  $i = 1, 2, \dots, n$  do
5:       for  $j = 1, 2, \dots, N$  do
6:         Sample  $u_{ij}$  from  $f(u | t_i)$ 
7:         Compute  $c_{ij} \leftarrow c_\psi(y_k, u_{ij} | t)$ 
8:       end for
9:     end for
10:    Compute  $w_k \leftarrow \frac{1}{nN} \sum_{ij} c_{ij}$ 
11:  end for
12:  return  $\frac{1}{M} \sum_k \nu(y_k) w_k$ 
13: end function
14: Return  $\tau(\text{ComputeMean}(t_1, \psi), \text{ComputeMean}(t_2, \psi))$ 

```

A.2 Derivation of Algorithm 1

Since we have Equation 10 and 11, furthermore, we can write

$$E[v(Y) | do(t)] = \iint v(y) f(y | \tilde{y}) w_\psi(\tilde{y}, t) f(\tilde{y} | t) d\tilde{y} dy, \quad (50)$$

where $w_\psi(\tilde{y}, t) \approx \frac{1}{|\mathcal{T}|} \sum_{t_i \in \mathcal{T}} \left[\int c_\psi(F_{\tilde{Y}|t}(\tilde{y}), F_{U|t}(u) | t) f(u | t_i) du \right]$. To verify Algorithm 1, we only need to show that

$$\int f(\tilde{y} | t, u) f(u | t_i) du \sim N(\gamma^T(\mu_{u|t_i} - \mu_{u|t}), 1), \quad (51)$$

where $f(\tilde{y} | t, u) = f(\tilde{y} | t) c_\psi(F_{\tilde{Y}|t}(\tilde{y}), F_{U|t}(u) | t)$. According to Equation 13 and 14, we know that

$$f(u | t_i) \sim N(\mu_{u|t_i}, \Sigma_{u|t}), \quad (52)$$

$$f(\tilde{y} | t, u) \sim N(\gamma^T(u - \mu_{u|t}), \sigma_{\tilde{y}|t,u}^2). \quad (53)$$

By integrating out the U , we have

$$\int f(\tilde{y} | t, u) f(u | t_i) du = \frac{1}{\sqrt{2\pi(\sigma_{\tilde{y}|t,u}^2 + \gamma^T \Sigma_{u|t} \gamma)}} \exp \left\{ -\frac{(y - \gamma'(\mu_{u|t_i} - \mu_{u|t}))^2}{2(\sigma_{\tilde{y}|t,u}^2 + \gamma^T \Sigma_{u|t} \gamma)} \right\}, \quad (54)$$

where $\sigma_{\tilde{y}|t,u}^2 + \gamma^T \Sigma_{u|t} \gamma = 1$.

A.3 Proof of Theorem 1

Theorem 1. Assume model 13-15. Let $[\psi_T] = \{\tilde{\psi}_T = \{A\mu_{u|t}, A\Sigma_{u|t}A\} : A \in \mathcal{S}^+\}$ where \mathcal{S}^+ is the space of symmetric positive definite matrices. Then $[\psi_T]$ is a causal equivalence class.

Proof. The intervention distribution for \tilde{y} is defined as

$$f_{\psi}(\tilde{y} \mid do(t)) = \int \left[\int f_{\psi_Y}(\tilde{y} \mid t, u) f_{\psi_T}(u \mid \tilde{t}) du \right] f(\tilde{t}) d\tilde{t} \quad (55)$$

where $\psi_Y = \gamma$ and $\psi_T = \{\mu_{u|t}, \Sigma_{u|t}\}$. Then, $\int f_{\gamma}(\tilde{y} \mid t, u) f_{\psi_T}(u \mid \tilde{t}) du \sim N(\gamma^T(\mu_{u|\tilde{t}} - \mu_{u|t}), 1)$ for any γ such that $\gamma^T \Sigma_{u|t} \gamma \leq 1$ (see Equation 54). Let $\tilde{\psi}_T = \{A\mu_{u|t}, A\Sigma_{u|t}A\} \in [\psi_T]$ where $A \in \mathcal{S}^+$ is a positive definite matrix and assume $\tilde{\psi}_Y = \tilde{\gamma}$. Then,

$$\int f_{\tilde{\gamma}}(\tilde{y} \mid t, u) f_{\tilde{\psi}_T}(u \mid \tilde{t}) du \sim N(\tilde{\gamma}^T A(\mu_{u|\tilde{t}} - \mu_{u|t}), 1). \quad (56)$$

Let $\tilde{\gamma} = A^{-1}\gamma$ be a bijective mapping from γ to $\tilde{\gamma}$. For any γ and positive definite A , we have $\tilde{\gamma}^T A \Sigma_{u|t} A \tilde{\gamma} = \gamma^T \Sigma_{u|t} \gamma \leq 1$ so that $\tilde{\gamma}$ is a valid copula parameter. In addition, $\int f_{\gamma}(\tilde{y} \mid t, u) f_{\psi_T}(u \mid \tilde{t}) du = \int f_{\tilde{\gamma}}(\tilde{y} \mid t, u) f_{\tilde{\psi}_T}(u \mid \tilde{t}) du$, which implies $f_{\gamma, \psi_T}(\tilde{y} \mid do(t)) = f_{\tilde{\gamma}, \tilde{\psi}_T}(\tilde{y} \mid do(t))$. Since Y is a deterministic function of \tilde{Y} , this implies $f_{\gamma, \psi_T}(y \mid do(t)) = f_{\tilde{\gamma}, \tilde{\psi}_T}(y \mid do(t))$. Therefore, $[\psi_T]$ is a causal equivalence class.

A.4 Proof of Theorem 2

Theorem 2. *Suppose that the observed data is generated by model 17-19. When there k treatments with $1 < m < k$, then ψ_T is identified up to the causal equivalence class $[\psi_T] = \{\psi_T = \{A\mu_{u|t}, A\Sigma_{u|t}A\} : A \in \mathcal{S}^+\}$. When there is a single treatment ($k = 1$) or $m = k$ confounders, then ψ_T is not identifiable up to causal equivalence class.*

Proof. The sample covariance matrix of the treatments is a consistent estimator for $B\Sigma_u B' + \sigma_{t|u}^2 I_k$, the covariance matrix T . As long as $1 < m < k$, then the k th eigenvalue is a consistent estimator for $\sigma_{t|u}^2$. $B\Sigma_u B'$ is identified by the m eigenvectors and eigenvalues of the sample covariance matrix. The span of the first m eigenvectors of the sample covariance matrix is a consistent estimator for the span of B . With model 17-19, the conditional distribution of confounder U

$$f(u \mid t) \sim N(\mu_{u|t}, \Sigma_{u|t}), \quad (57)$$

where $\mu_{u|t} := \Sigma_u B' (B\Sigma_u B' + \sigma_{t|u}^2 I_k)^{-1} t$, $\Sigma_{u|t} := \Sigma_u - \Sigma_u B' (B\Sigma_u B' + \sigma_{t|u}^2 I_k)^{-1} B \Sigma_u$, and the intervention distribution

$$f_{\gamma, B, \Sigma_u}(y \mid do(T = t)) \sim N((\tau_{\text{naive}} - (B\Sigma_u B' + \sigma_{t|u}^2 I_k)^{-1} B \Sigma_u \gamma)' t, \sigma_{y|t, u}^2 + \gamma^T \Sigma_u \gamma), \quad (58)$$

where all m -vectors γ which satisfy $\gamma^T \Sigma_{u|t} \gamma \leq \sigma_{y|t}^2$ are valid sensitivity parameters.

Let $\tilde{B} = BA$ and $\tilde{\Sigma}_u = A^{-1} \Sigma_u A^{-T}$ for an arbitrary positive definite matrix A , so that $\tilde{B} \tilde{\Sigma}_u \tilde{B}' + \sigma_{t|u}^2 I_k = B \Sigma_u B' + \sigma_{t|u}^2 I_k$. Then, the observed treatments are consistent with $T = \tilde{B} \tilde{U} + \epsilon_{t|u}$, where $\tilde{U} = A^{-1} U \sim N_m(0, \tilde{\Sigma}_u)$. Hence, the conditional confounder distribution

$$f(\tilde{u} \mid t) \sim N_m(\tilde{\mu}_{u|t}, \tilde{\Sigma}_{u|t}), \quad (59)$$

where $\tilde{\mu}_{u|t} = A^{-1} \mu_{u|t}$ and $\tilde{\Sigma}_{u|t} = A^{-1} \Sigma_{u|t} A^{-T}$. With \tilde{B} and $\tilde{\Sigma}_u$, the intervention distribution can be alternatively expressed as

$$f_{\tilde{\gamma}, \tilde{B}, \tilde{\Sigma}_u}(y \mid do(T = t)) \sim N((\tau_{\text{naive}} - (\tilde{B} \tilde{\Sigma}_u \tilde{B}' + \sigma_{t|u}^2 I_k)^{-1} \tilde{B} \tilde{\Sigma}_u \tilde{\gamma})' t, \sigma_{y|t, u}^2 + \tilde{\gamma}^T \tilde{\Sigma}_u \tilde{\gamma}) \quad (60)$$

with $\tilde{\gamma}$ satisfying $\tilde{\gamma}^T \tilde{\Sigma}_{u|t} \tilde{\gamma} \leq \sigma_{y|t}^2$ to be valid sensitivity parameter.

Let $\tilde{\gamma} = A^T \gamma$. If $\gamma^T \Sigma_{u|t} \gamma \leq \sigma_{y|t}^2$, then we have $\tilde{\gamma}^T \tilde{\Sigma}_{u|t} \tilde{\gamma} = \gamma^T \Sigma_{u|t} \gamma \leq \sigma_{y|t}^2$ and $f_{\tilde{\gamma}, \tilde{B}, \tilde{\Sigma}_u}(y | do(T = t)) = f_{\gamma, B, \Sigma_u}(y | do(T = t))$. Therefore, the causal equivalence class characterized by $\psi_T = \{\mu_{u|t}, \Sigma_{u|t}\}$ is identifiable when $1 < m < k$.

A.5 Proof of Theorem 3 and 4

Proof of Theorem 3

Theorem 3. *Suppose that the observed data is generated by model 17-19. Then, $\forall \gamma$ satisfying Assumptions 1 and 2,*

$$\gamma^T \Sigma_{u|t} \gamma \leq \sigma_{y|t}^2 R_{Y \sim U|T}^2, \quad (61)$$

For any given Δt , we have

$$Bias_{\Delta t}^2 \leq \sigma_{y|t}^2 R_{Y \sim U|T}^2 \|\Sigma_{u|t}^{-1/2} \mu_{u|\Delta t}\|_2^2, \quad (62)$$

The bound is achieved when γ is colinear with $\Sigma_{u|t}^{-1} \mu_{u|\Delta t}$.

Proof. Under model 17-19, the variance of the observed outcome equals

$$\begin{aligned} \sigma_{y|t}^2 &:= Var(Y | T) \\ &= \sigma_{y|t,u}^2 + \gamma^T (I_m - B^T (BB^T + \sigma_{t|u}^2 I_k)^{-1} B) \gamma \\ &= \sigma_{y|t,u}^2 + \gamma^T \Sigma_{u|t} \gamma, \end{aligned} \quad (63)$$

where $\gamma^T \Sigma_{u|t} \gamma$ corresponds to the confounding variation, and $\sigma_{y|t,u}^2$ stands for the non-confounding variation in the residual of observed outcome. Hence, the fraction of confounding variation in the residual of Y , $R_{Y \sim U|T}^2$, can be expressed in terms of equation 31, which produces a constrain for γ (equation 32) that the confounding variation in the residual of Y , $\gamma^T \Sigma_{u|t} \gamma$, should not be larger than $\sigma_{y|t}^2 R_{Y \sim U|T}^2$ for a given level of $R_{Y \sim U|T}^2$.

Let

$$Z := \Sigma_{u|t}^{1/2} \gamma, \quad (64)$$

then the omitted variable bias in equation 26 can be written as

$$Bias_{\Delta t} = Z^T \Sigma_{u|t}^{-1/2} \mu_{u|\Delta t},$$

where $Z^T Z \leq \sigma_{y|t}^2 R_{Y \sim U|T}^2$, implied by inequality 32.

Therefore,

$$Bias_{\Delta t}^2 = Z^T \Sigma_{u|t}^{-1/2} \mu_{u|\Delta t} \mu_{u|\Delta t}^T \Sigma_{u|t}^{-1/2} Z \quad (65)$$

$$\leq \sigma_{y|t}^2 R_{Y \sim U|T}^2 \|\Sigma_{u|t}^{-1/2} \mu_{u|\Delta t}\|_2^2, \quad (66)$$

where the bounds are reached when Z is colinear with $\Sigma_{u|t}^{-1/2} \mu_{u|\Delta t}$, i.e., γ is colinear with the $\Sigma_{u|t}^{-1} \mu_{u|\Delta t}$ inferred by the relationship defined in equation 64.

Corollary 3.1. *Let d_1 be the largest singular value of B . For all Δt with $\|\Delta t\|_2 = 1$, the squared bias is*

bounded by

$$\text{Bias}_{\Delta t}^2 \leq \frac{d_1^2}{(d_1^2 + \sigma_{t|u}^2)} \frac{\sigma_{y|t}^2}{\sigma_{t|u}^2} R_{Y \sim U|T}^2, \quad (67)$$

with equality when $\Delta t = u_1^B$, the first left singular vector of B . When $\Delta t \in \text{Null}(B')$, the naive estimate is unbiased, that is, $\text{PATE}_{\Delta t} = \tau'_{naive} \Delta t$.

Proof. Suppose that the matrix B has the singular value decomposition,

$$B = UDV^T,$$

where the diagonal entries of D are the singular values of B in descending order. Then, we can write

$$\mu_{u|\Delta t} = VD(D^2 + \sigma_{t|u}^2 I_s)^{-1} U^T \Delta t, \quad (68)$$

and

$$\Sigma_{u|t}^{-1} = V[I_s + \frac{1}{\sigma_{t|u}^2} D^2] V^T. \quad (69)$$

By plugging Equation 68 and 69 into the result of theorem 3, we have

$$\text{Bias}_{\Delta t}^2 \leq \frac{\sigma_{y|t}^2}{\sigma_{t|u}^2} R_{Y \sim U|T}^2 \|VD(\sigma_{t|u}^2 I_s + D^2)^{-1/2} U^T \Delta t\|_2^2, \quad (70)$$

where, according to Rayleigh quotient (Horn, 1985), the squared L2 norm reaches its maximum, $\frac{d_1^2}{(d_1^2 + \sigma_{t|u}^2)}$, when Δt equals the first column of U , i.e., the first left singular vector of B .

Therefore, we have

$$\text{Bias}_{\Delta t}^2 \leq \frac{d_1^2}{(d_1^2 + \sigma_{t|u}^2)} \frac{\sigma_{y|t}^2}{\sigma_{t|u}^2} R_{Y \sim U|T}^2. \quad (71)$$

Proof of Theorem 4

Theorem 4. Assume the model 13-15 with Gaussian outcomes. If $\Sigma_{u|t}$ is non-invertible, then Bias_{t_1, t_2} is bounded if and only if $\mu_{u|t_1} - \mu_{u|t_2}$ is in the row space of $\Sigma_{u|t}$. When bounded,

$$\text{Bias}_{t_1, t_2}^2 \leq \sigma_{y|t}^2 R_{Y \sim U|T}^2 \|(\Sigma_{u|t}^\dagger)^{1/2} (\mu_{u|t_1} - \mu_{u|t_2})\|_2^2, \text{ where } \Sigma_{u|t}^\dagger \text{ is the pseudo-inverse of } \Sigma_{u|t}.$$

Proof. Under model 13-15, we have $\gamma^T \Sigma_{u|t} \gamma + \sigma_{y|t, u}^2 = 1$, where $\gamma^T \Sigma_{u|t} \gamma$ corresponds to the confounding variation and $\sigma_{y|t, u}^2$ corresponds to the non-confounding variation in the Gaussianized Y . Therefore, the confounding variation, $\gamma^T \Sigma_{u|t} \gamma$ should not be larger than a given level of $R_{Y \sim U|T}^2$,

$$\gamma^T \Sigma_{u|t} \gamma \leq R_{Y \sim U|T}^2 \quad (72)$$

where $R_{Y \sim U|T}^2$ denotes the fraction of confounding variation in residual variance of \tilde{Y} conditional on T ⁴.

Let

$$Z := \Sigma_{u|t}^{1/2} \gamma, \quad (73)$$

⁴ $R_{Y \sim U|T}^2$ coincides with $R_{Y \sim U}^2$ here, but we use notation $R_{Y \sim U|T}^2$ for consistency.

then the omitted variable bias,

$$\text{Bias}_{t_1, t_2} = \sigma_{y|t} Z^T (\Sigma_{u|t}^\dagger)^{1/2} (\mu_{u|t_1} - \mu_{u|t_2}), \quad (74)$$

where $Z^T Z \leq R_{Y \sim U|T}^2$, implied by inequality 72.

Therefore,

$$\text{Bias}_{t_1, t_2}^2 = \sigma_{y|t}^2 Z^T (\Sigma_{u|t}^\dagger)^{1/2} (\mu_{u|t_1} - \mu_{u|t_2}) (\mu_{u|t_1} - \mu_{u|t_2})^T (\Sigma_{u|t}^\dagger)^{1/2} Z \quad (75)$$

$$\leq \sigma_{y|t}^2 R_{Y \sim U|T}^2 \| (\Sigma_{u|t}^\dagger)^{1/2} (\mu_{u|t_1} - \mu_{u|t_2}) \|_2^2, \quad (76)$$

where the bounds are reached when Z is colinear with $(\Sigma_{u|t}^\dagger)^{1/2} (\mu_{u|t_1} - \mu_{u|t_2})$, i.e., γ is colinear with the $\Sigma_{u|t}^\dagger (\mu_{u|t_1} - \mu_{u|t_2})$.

Suppose that $\Sigma_{u|t}$ has the eigendecomposition,

$$\Sigma_{u|t} = Q \Lambda Q^T, \quad (77)$$

where Q is the square $s \times s$ matrix whose j th column is the eigenvector q_j of $\Sigma_{u|t}$, and Λ is the diagonal matrix whose diagonal elements are the corresponding eigenvalues, $\Lambda_{jj} = \lambda_j$, in descending order. If $\Sigma_{u|t}$ is non-invertible and has rank p ($p \leq s$), then we have $\lambda_j = 0$ for $j = p + 1, \dots, s$.

On the one hand, when $\mu_{u|t_1} - \mu_{u|t_2}$ is in the row space of $\Sigma_{u|t}$, it can be expressed as a linear combination of q_j , $\sum_{j=1}^p a_j q_j$, $a_j \in \mathbb{R}$. Then, we have the squared omitted variable bias

$$\text{Bias}_{t_1, t_2}^2 \leq \sigma_{y|t}^2 R_{Y \sim U|T}^2 \| (\Sigma_{u|t}^\dagger)^{1/2} (\mu_{u|t_1} - \mu_{u|t_2}) \|_2^2, \quad (78)$$

$$= \sigma_{y|t}^2 R_{Y \sim U|T}^2 \| Q (\Lambda^\dagger)^{1/2} Q^T \sum_{j=1}^p a_j q_j \|_2^2, \quad (79)$$

$$= \sigma_{y|t}^2 R_{Y \sim U|T}^2 \sum_{i=1}^s \left(\sum_{j=1}^p a_j \lambda_j^{-\frac{1}{2}} Q_{ij} \right)^2, \quad (80)$$

where Q_{ij} denotes the element at the i th row and j th column of matrix Q , and Λ^\dagger is the pseudo-inverse of Λ by taking the reciprocal of each its non-zero element on the diagonal, leaving the zeros in place.

On the other hand, when Bias_{t_1, t_2}^2 is bounded, let's assume that $\mu_{u|t_1} - \mu_{u|t_2}$ is not in the row space of $\Sigma_{u|t}$, say $\mu_{u|t_1} - \mu_{u|t_2} = q_s$. Since $\lambda_s = 0$, $\lambda_s^{-1/2} = \infty$ so as the bound of Bias_{t_1, t_2}^2 equal to ∞ , which contradicts the condition that Bias_{t_1, t_2}^2 is bounded.

Therefore, Bias_{t_1, t_2}^2 is bounded if and only if $\mu_{u|t_1} - \mu_{u|t_2}$ is in the row space of $\Sigma_{u|t}$.

B Modeling Choice Details

B.1 Identification and Inference in the Factor Model

Here, we briefly elaborate on identifiability of the probabilistic principal components model, which is a prerequisite for our multi-cause sensitivity analysis. Identifiability under various factor model assumptions is well studied and has a long history in the literature (Mardia et al., 1980; Everett, 2013). In the specific probabilistic principal components model 18, Tipping and Bishop (1999) provide a maximum likelihood solution for inferring the latent confounder parameters conditional on m . Many procedures are available for selecting the appropriate value of m , using for example Bayesian model selection techniques (Minka, 2001)

or large p , small n asymptotics [Gavish and Donoho \(2014\)](#).

The change of variables described at the end of the subsection [5.1](#) further elucidates important situations in which we cannot bound the omitted variable bias due to non-identifiability of the factor model. Again, we focus on the rotated treatments $\tilde{T} \sim N(0, \Delta + \sigma_{t|u}^2 I_k)$ and highlight two simple situations in which we cannot bound the causal effects. First, when B is rank k , i.e. there exist $m = k$ independent confounders, Δ has no non-zero entries on the diagonal and thus we cannot identify either Δ nor $\text{Cov}(\epsilon_{t|u}) = \sigma_{t|u}^2 I_k$, only their sum. Second, if $\text{Cov}(\epsilon_{t|u})$ is an unknown arbitrary diagonal matrix (as opposed to a matrix proportional to the identity), then $\text{Cov}(\epsilon_{t|u})$ is not distinguishable from Δ . In both of these cases, the worst-case bias is unbounded since the non-confounding variation of the treatment assignment, $\text{Cov}(\epsilon_{t|u})$, can be arbitrarily small. In such settings, we can still apply approaches used in single cause sensitivity analysis, by specifying both Ψ_Y and Ψ_T ; when the factor model is not identifiable, Ψ_T must be chosen as a true parameter, e.g. by bounding the fraction of treatment variation due to confounding, $R_{T \sim U}^2$.

B.2 Confounder Inference with Variational Autoencoders

Probabilistic Principal Component Analysis should only be used when the treatments are approximately Gaussian treatments. For binary and other general treatment distributions, more sophisticated probabilistic latent variables models are required. Examples of such latent variable models include models for count data like the logistic factor analysis ([Hao et al., 2015](#)) and Poisson factor analysis methods ([Gopalan et al., 2013](#)). Unfortunately, these models imply posteriors which are non-Gaussian and heteroskedastic, violating Assumptions [5](#) and [4](#).

As such, for general treatment distributions, our approach is to infer a conditional Gaussian latent variable model using a variational autoencoder (VAE). VAEs have been extremely popular in machine learning, in particular for generating low dimensional representations of complex inputs like images ([Pu et al., 2016](#)) but more recently have been used in scientific and decision-making applications ([Lopez et al., 2020](#)) and in applications to causal inference ([Louizos et al., 2017](#)). A VAE consists of a prior distribution, $f(u)$, typically for the low-dimensional latent variables, a stochastic encoder, and a stochastic decoder. In our application, the inferred stochastic decoder, $\hat{f}_\theta(t | u)$, is a non-linear map from latent confounders to a distribution over causes. Together, the prior distribution for u and the decoder imply a posterior confounder distribution, $\hat{f}(u | t)$.

In practice, inference for the true posterior is intractable and so a variational approximation, called the encoder, $q_\phi(u | t)$, is used in place of the true posterior. Typically the encoder is chosen to be a normal distribution with mean and variance which are non-linear functions of the input, $q_\phi = N(\mu_\phi(t), \sigma_\phi^2(t))$. A crucial question is that how well the Gaussian encoder approximates the true posterior; improving the variational approximation to the true latent variable posterior is an area of active research. In this work, we follow a common strategy of using the encoder learned by the VAE as the proposal distribution in an importance sampler ([Lopez et al., 2020](#)).

Specifically, we apply a variant of the Constant-Variance Variational Autoencoder (CV-VAE) ([Ghosh et al., 2020](#)) to infer the conditional confounder distribution, $f(u | t) \sim N(\mu_{u|t}, \Sigma_{u|t})$, in which $\Sigma_{u|t}$ does not depend on the level of t . We use the importance sampling to improve estimates of the conditional mean $\mu_{u|t}$, and posterior variance, $\Sigma_{u|t}$. While this approach only yields an approximation to the true posterior, we demonstrate the practical effectiveness of this approach in Sections [7](#) and [8](#).

B.3 Binary Outcomes

For binary outcomes with the risk ratio estimand:

$$RR_{t,\cdot} = \sum_{t_i \in \mathcal{T}} \Phi(\Phi^{-1}(\mu_{y|t}) + \gamma^T(\mu_{u|t_i} - \mu_{u|t})) \Big/ Pr(Y = 1), \quad (81)$$

which implies that

$$RR_{t_1, t_2} = \sum_{t_i \in \mathcal{T}} \Phi(\Phi^{-1}(\mu_{y|t_1}) + \gamma^T(\mu_{u|t_i} - \mu_{u|t_1})) \Big/ \sum_{t_i \in \mathcal{T}} \Phi(\Phi^{-1}(\mu_{y|t_2}) + \gamma^T(\mu_{u|t_i} - \mu_{u|t_2})), \quad (82)$$

where $\gamma^T \Sigma_{u|t} \gamma \leq \sigma_{\tilde{y}|t}^2 R_{\tilde{Y} \sim U|T}^2$. We can numerically explore values of RR_{t_1, t_2} within the valid domain of γ , and calculate the corresponding implicit partial R-squared by $R_{\tilde{Y} \sim U|T}^2 = \frac{\gamma^T \Sigma_{u|t} \gamma}{\sigma_{\tilde{y}|t}^2}$. To calculate the robustness value, we only need to find the value of $R_{\tilde{Y} \sim U|T}^2$ for which the corresponding $RR_{t_1, t_2} = 1$. Noticeably, RR_{t_1, t_2} is not monotone in $R_{\tilde{Y} \sim U|T}^2$, since the variance of intervention distribution also depends on γ . This is evident in the simulation in Section 7 where we fit the observed outcome model by probit regression and the valid range for scalar γ is $[-\frac{1}{\sigma_{u|t}}, \frac{1}{\sigma_{u|t}}]$. We visualize the non-monotone relationship between RR_{t_1, t_2} and $R_{\tilde{Y} \sim U|T}^2$ in Figure 7.

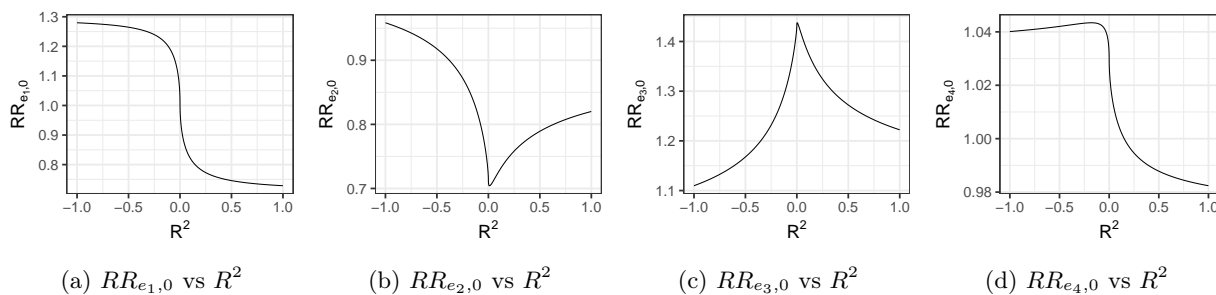


Figure 7: RR_{t_1, t_2} is non-monotone in $R_{\tilde{Y} \sim U|T}^2$. Positive values of R^2 indicates that U is positively correlated with \tilde{Y} , and negative values of R^2 means that U is negatively correlated with \tilde{Y} .

C Additional Results

C.1 Additional Results from Simulation in Sparse Effects Setting

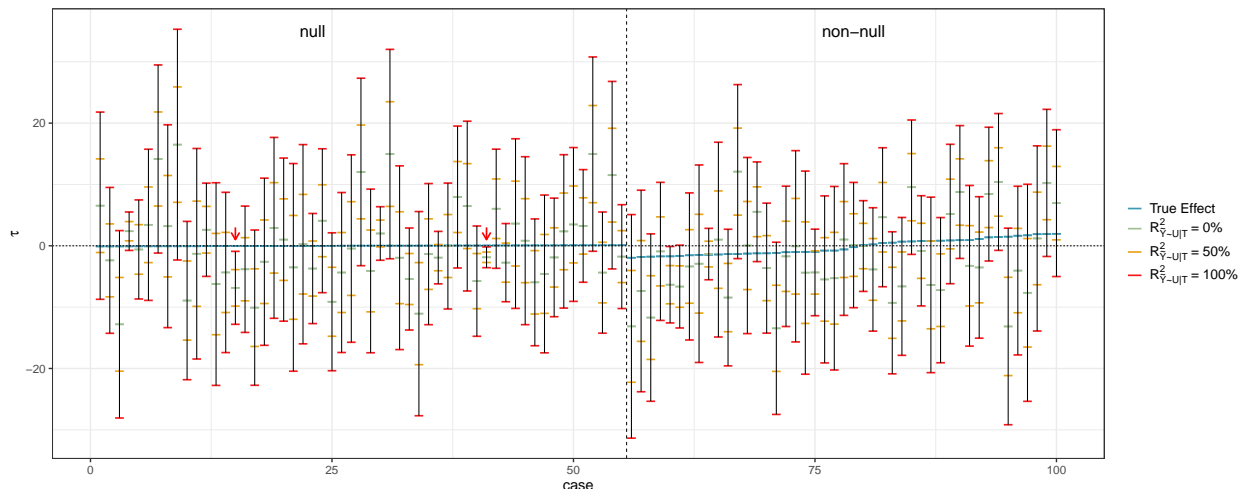


Figure 8: Worst-case ignorance regions for 55 randomly chosen null effects (left) and all 45 non-null effects (right) ordered by the magnitude of true effects in each group. Two red arrows indicate non-null treatments for which the worst-case ignorance region does not cover the true effect. This appears to be due to estimation error in the outcome model, more so than with the VAE.

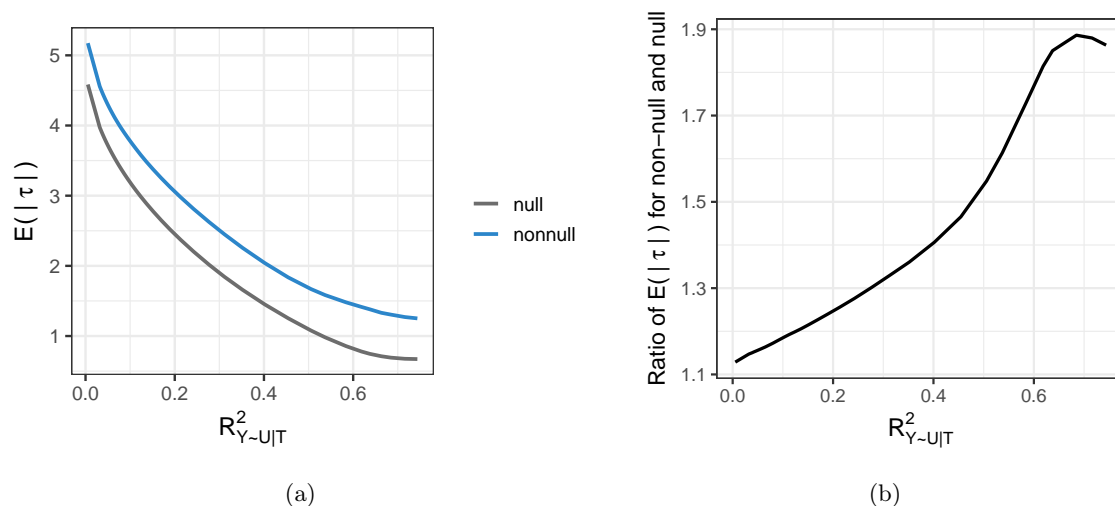


Figure 9: Change in $E(|\tau|)$ for the L1-minimized estimates as a function of $R^2_{Y \sim U|T}$, separated by null and non-null effects. (a) The magnitude of effects decreases with \mathcal{R}^2 , with a larger relative decrease for null contrasts. (b) The relative magnitude of non-null and null effects increases with \mathcal{R}^2 in general. The magnitude of non-null effects can be as large as 1.9 times the null effects when \mathcal{R}^2 is large.

C.2 Additional Results from the Actor Case Study

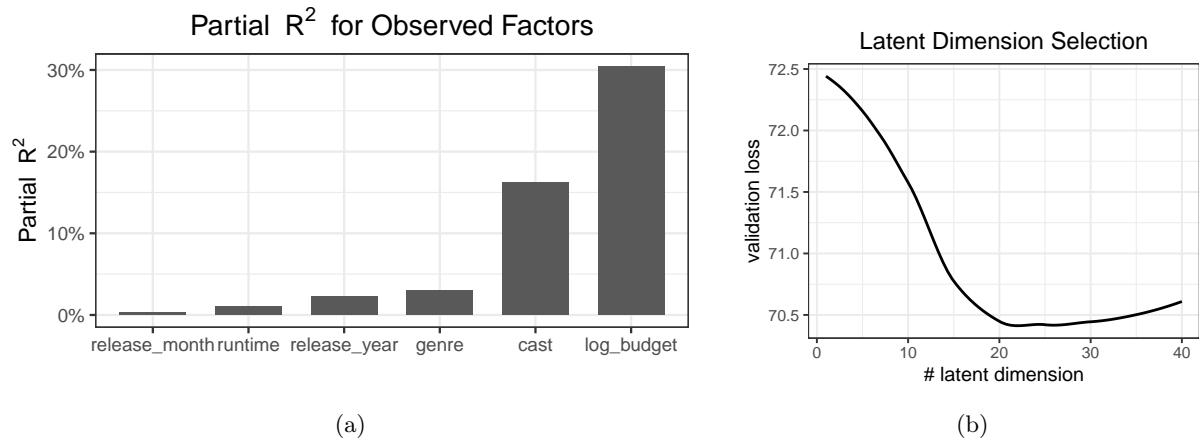


Figure 10: (a) Estimated partial R^2 for observed confounders using method described in section 6.1. Budget is the most dominant variable, which can explain significantly higher variation in outcome Y . (b) Latent confounder dimension selection, based on the reconstruction loss on the validation set.

Table 1: Robustness Value for Significant Actors

	Effect	$RV_{mean}(\%)$	$RV_{limit}(\%)$
John Ratzenberger	52.91	21.79	9.36
Tom Cruise	49.48	5.09	1.59
Stan Lee	47.53	14.43	4.16
Morgan Freeman	41.95	1.63	0.26
Will Smith	41.87	8.61	2.64
Bruce Willis	41.44	1.86	0.3
Tom Hanks	36.40	4.16	0.79
Harrison Ford	35.26	3.25	0.6
Arnold Schwarzenegger	34.13	3.39	0.55
Johnny Depp	31.53	1.27	0.08
Frank Welker	30.99	2.86	0.34
Brad Pitt	30.61	1.54	0.09
Judi Dench	30.01	8.87	1.41
Leonardo DiCaprio	29.52	36.47	7.35
Adam Sandler	28.39	3.22	0.19
Liam Neeson	27.40	0.91	0.03
Denzel Washington	26.09	2.01	0.11
Eddie Murphy	25.82	3.30	0.27
John Travolta	23.96	2.45	0.13
Robin Williams	23.26	1.12	0.03
Hugo Weaving	23.02	4.20	0.12
Michael Caine	22.23	3.03	0.11
Channing Tatum	22.22	2.33	0.06
Angelina Jolie	20.81	3.72	0.09
Carla Gugino	20.74	4.24	0.13
Octavia Spencer	20.68	5.78	0.13
Kathy Bates	20.58	8.25	0.17
Jim Carrey	19.79	2.79	0
Ian McKellen	19.02	4.70	0
Reese Witherspoon	18.97	8.17	0.27
Zoe Saldana	18.79	7.33	0.12
Kevin Hart	18.41	3.21	0.05
Timothy Spall	18.40	9.39	0.25
Jamie Foxx	18.15	6.02	0.01
Judy Greer	17.76	4.17	0.01
Tommy Lee Jones	17.67	2.96	0
Rose Byrne	16.85	7.62	0.05
Andy Serkis	16.53	9.48	0.05
Dennis Hopper	-14.79	19.32	0
Kate Bosworth	-16.01	5.20	0.04
Viggo Mortensen	-16.24	6.50	0.02
Tim Blake Nelson	-16.58	24.78	0.09
Jeremy Piven	-17.45	4.86	0.06
Elias Koteas	-21.64	13.87	1.06
Susan Sarandon	-22.57	7.90	0.24
Mark Ruffalo	-23.29	3.17	0.11